DESIGN OF VISCO-ACOUSTIC WAVEFIELD FINITE IMPULSE RESPONSE (FIR) EXTRAPOLATION FILTERS

BY

SYED ABDUL SALAM

A Thesis Presented to the
DEANSHIP OF GRADUATE STUDIES

KING FAHD UNIVERSITY OF PETROLEUM & MINERALS

DHAHRAN, SAUDI ARABIA

In Partial Fulfillment of the
Requirements for the Degree of

MASTER OF SCIENCE

In

ELECTRICAL ENGINEERING

DECEMBER 2015

KING FAHD UNIVERSITY OF PETROLEUM & MINERALS
DHAHRAN 31261, SAUDI ARABIA

DEANSHIP OF GRADUATE STUDIES

This thesis, written by **SYED ABDUL SALAM** under the direction of his thesis adviser and approved by his thesis committee, has been presented to and accepted by the Dean of Graduate Studies, in partial fulfillment of the requirements for the degree of **MASTER OF SCIENCE IN ELECTRICAL ENGINEERING.**

Thesis Committee

Dr. Wail A. Mousa
(Advisor)

Dr. Abdullatif A. Al-Shuhail
(Member)

Dr. Azzedine Zerguine
(Member)

Dr. Ali Ahmad Al-Shaikhi
Department Chairman

Dr. Salam A. Zummo
Dean of Graduate Studies

23/12/15
Date

Dedication

This thesis is dedicated to my family and in memory of my father.

ACKNOWLEDGMENTS

In the name of Allah, the most Gracious and the Most Merciful

Firstly, I would like to thank Allah who gave me such opportunity, courage and patience to carry out my research work and was able to complete my tasks within the required time.

Secondly, my deepest gratitude to my thesis Advisor Dr. Wail A. Mousa. He always encouraged me and provided me good solutions to the problems. His useful suggestions lead to successful research work. His previous research publications and MATLAB codes were also helpful for my thesis. Being his student, now i feel comfortable doing research in the field of seismic signal processing.

Thirdly, I also want to thank KFUPM and my thesis committee members. King Fahd University of Petroleums and Minerals (KFUPM) provided me funded scholarship for my M.Sc. Electrical Engineering. This financial assistance enabled me to do my research work. I want to thank my committee members Dr. Abdulatif A. Al-Shuhail and Dr. Azzedine Zerguine from KFUPM. Dr. Abdullatif provided me access to high performance computing lab along with other resources. Working with him in few projects helped me learning the concepts of geophysics. Dr. Azzedine Zerguine provided me solid background in the course Adaptive

Filtering/Applications. These concepts were helpful in my thesis work.

I also want to thank my mother, siblings, my grand parents and wife. Special thanks to my grand father, who always supported me financially. All of them prayed for my success and supported me during tough times.

Finally, I would like to thank Dr. Jan Thorbecke, who is working at Cray Company and also as researcher at Delft University of Technology, Netherlands. His opensource codes for forward modeling and prestack depth migration helped me in completing my research goals. I am also thankful for his quick replies to my emails. His Ph.D thesis was also helpful in understanding the concepts.

TABLE OF CONTENTS

LIST OF TABLES

LIST OF FIGURES

THESIS ABSTRACT

NAME: Syed Abdul Salam

TITLE OF STUDY: Design of Visco-Acoustic Wavefield Finite Impulse Response (FIR) Extrapolation Filters

MAJOR FIELD: Electrical Engineering

DATE OF DEGREE: December, 2015

Explicit depth frequency-space ($f-x$) prestack imaging is one of the attractive mechanisms of seismic imaging. So far the main focus of this method was migrating data assuming acoustic medium but very little work assumed visco-acoustic media. Real seismic data usually suffers from attenuation and dispersion effects. In order to compensate for the attenuation and dispersion in visco-acoustic medium, new operators are required. We propose using the L_1-norm and weighted L_1-error minimization techniques to design visco-acoustic $f-x$ extrapolators. L_1-norm is sparsity preserving so sparse extrapolators are designed. To show the accuracy and compensation of the operators, prestack depth migration is performed on the challenging Marmousi model for both acoustic and visco-acoustic datasets. The final migrated images show that the proposed L_1-norm extrapolation results

in practically stable images with improved resolution. The L_1-error provide even better results because it gives more weight to the important passband.

ملخص الرسالة

الاسم الكامل: سيد عبد السلام

عنوان الرسالة: تصميم فيسكو-الموجات الصوتية الميدان محدود دفعة الاستجابة (FIR) استقراء الفلاتر

التخصص: الهندسة الكهربائية

تاريخ الدرجة العلمية: ديسمبر ٢٠١٥

يعتبر التصوير العمقي الصريح المقام في مجال التردد-المسافة من أكثر اساليب التصوير الأرضي فاعلية. الافتراضية السائدة المستخدمة الى الان في هذا الأسلوب هي ان الأرض عبارة عن وسط صوتي مع وجود القليل من الاعمال التي تفترض بانها وسط صوتي لزج و ذلك على الرغم من ان الموجات السيزملوجية التي تستخدم في التصوير تعاني من الضعف و التشتت اثناء مرورها بطبقات الأرض، ما يعني بان الافتراض بانها وسط صوتي لزج ينتج عنه نتائج اكثر دقة. لأخذ هذه الافتراضية بعين الاعتبار, لابد من تصميم عوامل تصويرية تأخذ اثار هذه الافتراضية بعين الاعتبار. لقد قمنا بابتكار عوامل تصويرة في هذه الأطروحة لأخذ هذه الفرضية الأكثر دقة بعين الاعتبار عن طريق استخدام المعدل الإحصائي الأول و المعدل الإحصائي المرجح الأول للخطأ لتصميم هذه العوامل. يقوم المعدل الإحصائي الأول بأخذ تناثر أجزاء العوامل التصويرية و قرب بعضها من الصفر وهي خاصية تتمتع بها هذه العوامل بعين الاعتبار. لاختبار فاعلية هذه العوامل و دقتها في تصوير الطبقات الأرضية, تم اختبارها على نموذج يعتبر معيارا في التصوير الأرضي و المسمى بنموذج مارموزي " Marmousi Model". تم استخدام هذا النموذج مع كلتا الفرضيتين و تظهر النتائج الدقيقة ان الطريقة المقترحة تقوم بتصميم عوامل تصويرية مستقرة و دقيقة لتستخدم في التصوير الأرضي.

CHAPTER 1

INTRODUCTION

1.1 Introduction

Natural resources like oil, gas, coal and other minerals are important for life. These resources are buried inside earth (both land and marine). To explore these resources we need a clear image of the earth sub-surface [1]. This image can be obtained using method of reflection seismology. In this method, artificial seismic waves are generated and these waves are reflected from different geological layers which are recorded by receivers. The recorded data is in raw form and it needs further processing to obtain the image of earth sub-surface [1, 2].

Digital signal processing has played important role in many applications. Some examples are sonar, radar, medical, communications and seismology [3]. The actual application of signal processing in seismology began with the work of Geophysical Analysis Group at the Massachusetts Institute of Technology (MIT) in the era 1960-65, it was historical milestones in seismic data processing [4].

To obtain the image of earth subsurface some preprocessing is required to attenuate noise accompanying the data. By using an imaging technique, the time traces of the preprocessed shot records are transformed into depth traces. For this process a earth model is required and the imaging technique is called *migration*. After the imaging, a geologist can interpret the migrated section and can identify the layers and structures in the earth subsurface model. For instance, this interpretation can be used to make a decision about the position of a future borehole. If an error is made in the imaging technique and interpretation based on it is wrong, the borehole will miss its target. Therefore, a good quality of imaging technique (or seismic migration) is important.

Seimic Migration can be performed in different domains and in each domain there are number of algorithms. There exists many migration (extrapolation) algorithms. One migration method is frequency-wavenumber ($f - k_x$) algorithm [1, 5]. In this method the data in time-space $(t - x)$ domain is first transformed into frequency-wavenumber $(f - k_x)$ domain. At each frequency sample, a complex-valued FIR filters are applied in the wavenumber-response domain. Another method is frequency-space $(f - x)$, in which the data is transformed into frequency-space domain before migration, only the time axis is transformed to the frequency. In this method FIR extrapolation filters (known as extrapolators) are applied in space domain via convolution [5, 6, 7]. By using convolution, each designed filter output can be calculated independently (or in parallel). In addition, this method can easily be extended to 3-D depth migration. This method

can accurately migrate the one-way wavefields through strong laterally varying media.

Most of the existing methods focused on acoustic data migration, which is the best approximation of the earth subsurface. Many researchers used different approaches to design non-compensating acoustic medium wavefield extrapolators in the $f - x$ domain [6, 5, 8, 9, 7, 10, 11, 12, 13]. In reality, the wave attenuates as it travels in the earth. If data is considered to be visco-acoustic, then new methods are required to compensate for addressing the effect of attenuation and dispersion. The loss in energy, if not compensated, reduces the data resolution. Depth migration is considered to be a physically more consistent and accurate domain to compensate and improve the resolution of the data at higher depths [14, 15].

1.2 Contributions

As in reality, the data encounter attenuation. To compensate for this attenuation new operators are required. To verify the newly design FIR filters (which have compensating effect for attenuation) on shot records or prestack data sets, the following three main components are required:

- Acoustic and visco-acoustic data sets.
- Compensating visco-acoustic FIR filter designs.
- Prestack depth migration algorithm.

Firstly, we generated shot gathers for acoustic and visco-acoustic case. Acoustic data set is required to get a reference migrated image. Visco-acoustic data set is required to compare the results of compensating and non-compensating operators with that of reference migrated section. Secondly, visco-acoustic compensating operators are designed with two algorithms. First algorithm design is compensating L_1-norm (sparse and non-sparse) FIR filters and second design is weighted L_1-error compensating FIR filter designs. Finally, for verification, the prestack depth migration process is required. Prestack depth migration to our designed filters is used and the resulting images are provided.

1.3 Organization of Thesis

In chapter 2, the background of seismic data processing, migration and visco-acoustic concepts are discussed. In chapter 3, the compensating L_1-norm visco-acoustic $f - x$ filters (both sparse and non-sparse) are designed. The filters responses are shown along with prestack depth migration of Marmousi model data sets. In chapter 4, the method of weighted L_1-error is presented. The importance of weighting is discussed and the accuracy of the filters are shown along with the migrated sections. In the end of chapter both the algorithms of L_1-norm and weighted L_1-error are compared. In chapter 5, the final concluding remarks are presented. Also, further recommendations are suggested for possible future work.

CHAPTER 2

BACKGROUND

2.1 Introduction

Among many geophysical techniques, seismic reflection is the most widely used. Its success lies in the fact that the seismic raw data is used to generate migrated images of the earth's subsurface structures. Seismic signals are generated at a source (such as explosion) which propagates through different layers of the earth. These signals are reflected, refracted and lost (due to attenuation). At the surface, the reflected signals are recorded by receivers at the acoustic impedance contrast. Reflectivity defines the strength of the impedance contrast. The signals recorded by these receiver is termed as seismic raw data which is further processed to obtain the migrated images of the earth subsurface structures. This processing require several steps. The following are typical seismic signal processing steps [1]:

- Preprocessing
- Deconvolution

- CMP sorting
- Velocity analysis
- NMO correction and muting
- Stacking
- Migration

These steps are for poststack migration algorithms. In case of prestack migration, the stacking is done after migrating each independent shot gather.The primary steps in the above workflow are deconvolution, stacking and migration, rest are secondary processes and improve the performance of these primary stages. The function of primary steps are summarized as:

- Deconvolution: Increases the vertical/time resolution
- Stacking: Increases the signal to noise ratio and produces the initial subsurface image
- Migration: Increases the horizontal resolution and produces the final subsurface image

In this thesis the main focus is on migration which is the final stage of the workflow.

2.2 Migration

The earliest migration[1] technique were graphical and was based on geometrical ideas developed. In 1954 Hagedoorn describes the process of seismic migration in terms of propagating wavefronts and tries to avoid the use of non-physical ray paths [16]. Later on Huygens-Fresnel argued that the beam between source and receiver is at least a half wavelength wide, therefore, rather than rays it is better to work with propagating wavefronts. Huygens' principle is basis of migration [1, 17].

In seismic migration, wave propagation effects, can correctly determine the reflection points of the subsurface structures [18]. Migration can be defined as the process of reconstructing a seismic section so that the reflection events are repositioned under their correct surface location at their correct vertical reflection (time or depth) location [1, 19]. The migration process removes the distorting effects of dipping reflectors from the seismic sections. In addition it also removes the diffracted arrivals which are resulted from sharp lateral discontinuities [20, 21].

2.2.1 Migration Types

Migartion can be classified as poststack or prestack migration. In poststack migration, the migration process is done on the Common Midpoint gather (CMPs) stacked data set. In prestack migration, migration is performed either on CMPs or Common shot gathers (CSGs) and the migrated sections are stacked after mi-

[1]The collection of reprints of Gardner is recommended for complete overview of migration upto 1985

gration. Prestack migration is relatively expensive in terms of processing [22]. On the other hand, poststack migration is not that much expensive but less accurate in complicated sub-surfaces.

Migration can also be classified as depth and time migration. Both prestack and poststack migration can give output in time or depth. This classification is based on how much physics we put in the algorithm. For strong velocity variations, depth migration is used which results in depth section. Geological examples of strong lateral velocity variations include salt overhangs, sub-salt regions or its combination. In Figure 2.1, both the poststack and prestack migrations are compared based on the lateral velocity variations and complexity of the algorithm. Among all, the prestack depth migration results in good quality images of the sub-surface with strong lateral velocity variations at the expensive of processing power.

2.2.2 Two-way and one-way Migration

Two-way wavefields can be described in terms of total acoustic pressure and the total particle velocity. Both the terms are always coupled by the two-way wave equations. In one-way, the wavefields are described by the wave traveling in the positive and negative axial direction. If the parameters of the medium are not varying, the axial direction of up-going and down-going one-way wave are completely decoupled. If the medium parameters are varied, the coupling between both the waves is expressed in terms of axial variations of the medium parameters.

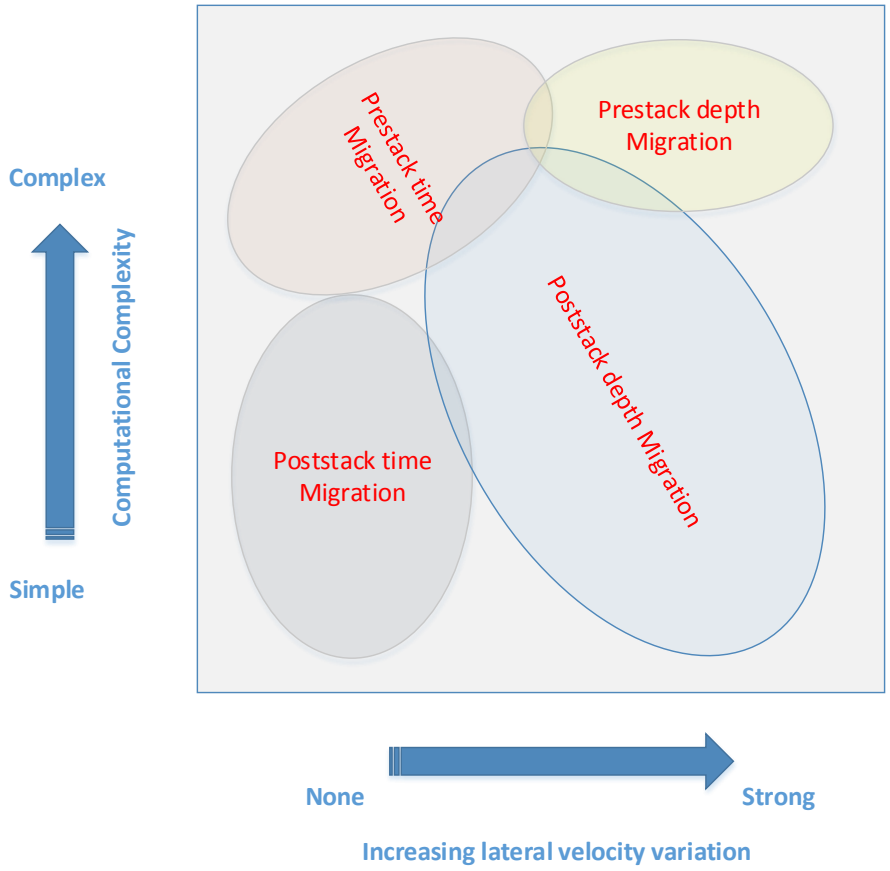

Figure 2.1: Types of migration based on lateral velocity variations and computational complexity.

In surface seismic exploration the vertical direction is preferred which makes the one-way wave theory well suited for seismic applications [7].

Migration can be implemented in number of ways. It is expensive process in terms of processing and the final step to the seismic reflection data to be interpreted. As it is considered the last major step in the seismic processing, so it is blamed for the problems with the earlier processing steps [22]. There are number of algorithms and different ways to classify the algorithms. Here, our algorithm depends on one-way extrapolation. In Figure 2.2, variety of different algorithms are shown for seismic reflection data. This hierarchy shows the assumptions made for solving initial partial differential equations. Algorithms are available in different domains like $f-x$, $f-k_x$. Frequency-wavenumber-space $f-k_x-x$ is called dual domain methods because this algorithm bounce back and forth in frequency, wavenumber and space.

2.2.3 Explicit $f-x$ Depth Extrapolation

Seismic imaging in the $f-x$ domain is among the attractive methods for imaging the earth subsurface structures [6, 5, 1]. This method is implemented via spatial convolution to obtain seismic images [23, 1], so each output sample can be computed independently, whenever parallel implementation is possible. Most importantly, one-way wave extrapolation in the $f-x$ domain can accurately image the subsurface with strong lateral varying medium. For strong varying medium, short length filters are required. Also, the short length filters will reduce

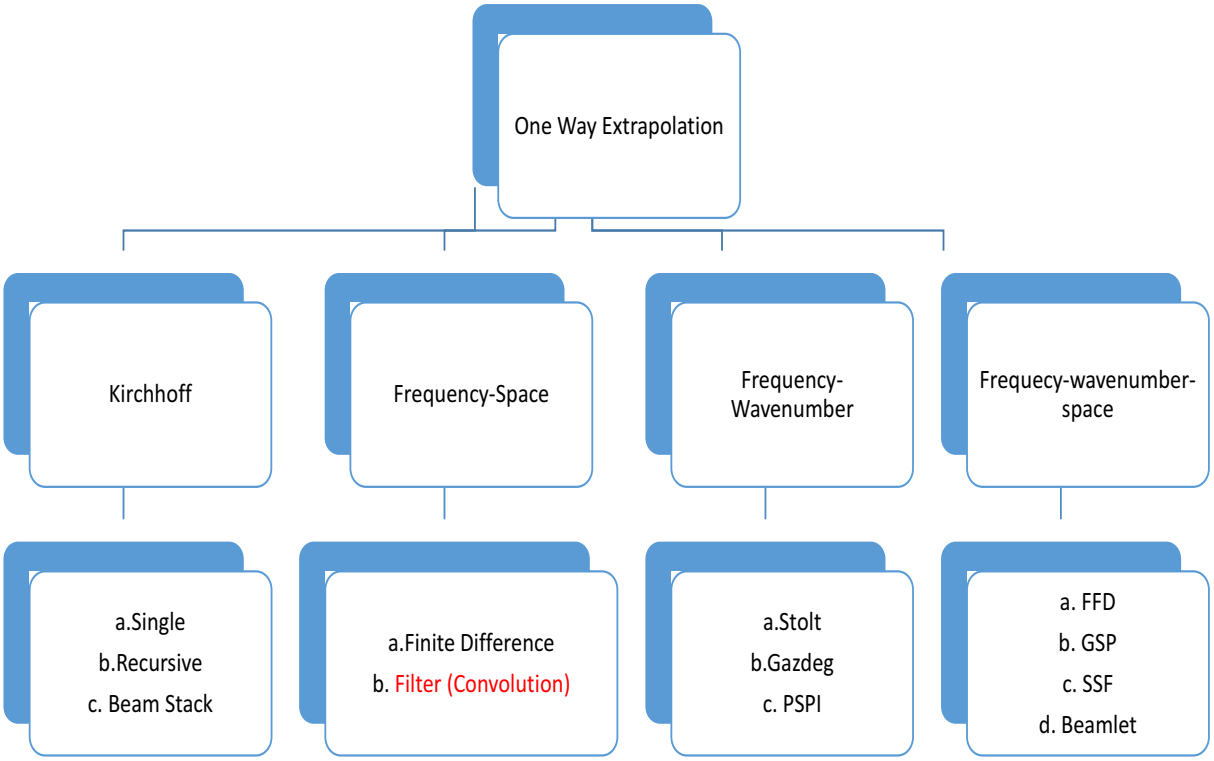

Figure 2.2: One-way extrapolation algorithms.

the computational cost of convolution. At the same time, to accommodate high propagation angles of wavefields, large length filters become desirable. Hence, the design problem can be treated as an optimization problem between the two trade-offs [10, 11].

The explicit $f-x$ migration can be easily extended to the 3-D depth migration, which requires 2-D filters as extrapolators. The $f-x$ extrapolation, can accurately image the laterally varying materials by using N length FIR digital filters. In the $f-x$ extrapolation, the seismic wavefields are spatially sampled, i.e. $u(x_i, e^{jw_r}, z_k)$ from depth z_k to $z_{k+1} = z_k + \triangle z$ and the process can be performed independently for each frequency w_r by spatial convolution with a pre-designed filter [24].

$$u(x_i, e^{jw_r}, z_{k+1}) = \sum_{n=(-N+1)/2}^{(N-1)/2} h[n]u(x_{i-n}, e^{jw_r}, z_k) \tag{2.1}$$

In equation 2.1, it is shown how to apply the designed $h[n]$ filter response to extrapolate for each depth level. In prestack extrapolation is applied to both downgoing and upgoing wavefields. This process is recursive in nature as shown by the equation 2.1. Due to this recursive nature of algorithm the extrapolation process can be unstable, so accurate designs are required to avoid instability. In the equation 2.1, $x_i = i\Delta x$ and $z_k = k\Delta z$ for all i and $k \in \mathbb{Z}$ (set of integers).. This method can be easily extended to 3-D Seismic Migration. When explicit depth migration is treated as filtering process it resembles convolution and we can compute each sample independently. This method is less expensive and can handle lateral variations in velocity.

2.2.4 Explicit $f - x$ Prestack Depth Migration

Prestack depth migration is a model-based seismic imaging methodology that works well for complex geological structures such as subsalt layers and basement fractures [25]. Prestack migration is results in better image quality, but at the expense of processing power. The method used for migration in this thesis is explicit $f - x$ prestack depth migration.

In this method, extrapolation in performed on each shot gather and stacking is done at later stage. While in poststack migration extrapolation is done on stacked section. Shot gather is first transformed from $t - x$ domain to $f - x$ domain. FIR filter is selected based on frequency (f), velocity (c) and value of Q. For each frequency, both downgoing and upgoing extrapolation is performed followed by imaging condition. This process is repeated for each depth step. When this process is completed for each depth level, this results in migrated image for one shot gather. The same process is repeated for all shot gathers. Once this process is completed for all shot gathers, stacking of all the migrated images is done to get the final migrated depth section. This algorithm is shown by Algorithm 1 and a flowchart in the Figure 2.3.

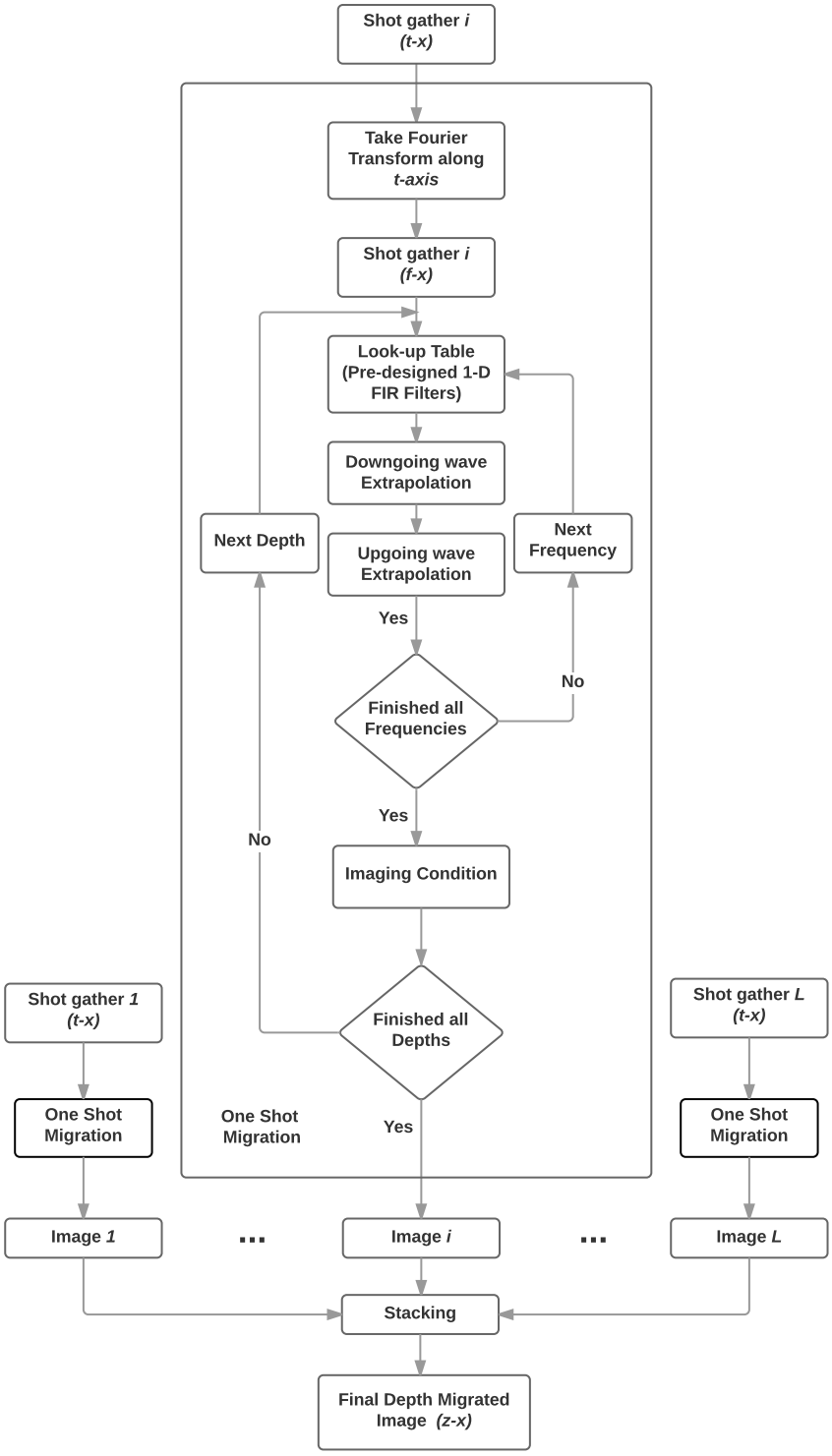

Figure 2.3: Explicit $f - x$ prestack depth migration process.

Algorithm 1 Explicit $f-x$ prestack depth migration

```
1: procedure PRESTACK
2:     for each shot gather do
       Input shot gather i in (t − x)
       Fourier transform of shot gather i along (t − axis)
       Shot gather i in (f − x)
3:       for each depth level do
4:           for each freqeuency do
       Look-up Table (Predesigned 1-D FIR Filters)
       Downgoing wave extrapolation
       Upgoing wave extrapolation
5:           end for
       Imaging Condition
6:       end for
       Image i
7:     end for
       Stacking
       Get the final depth migrated (z − x) section
8: end procedure
```

2.3 Visco-Acoustic Concepts

2.3.1 Linear Visco-Acoustic Medium

In frequency domain wave equation for linear visco-acoustic medium is given by

$$\{\partial_i^2 + \frac{\omega^2}{(M(\omega,x)/\rho)}\}P(\omega,x) = 0 \tag{2.2}$$

$$c(\omega,x) = \sqrt{M(\omega,x)/\rho}$$

at lateral position x and ω frequency, where $P(\omega,x)$ is pressure, $M(\omega)$ is bulk modulus, ∂_i^2 is partial differentiation with respect to cartesian coordinates and ρ is density. If velocity is independent of lateral coordinate i.e. x, spatial Fourier transform along x-direction is performed on equation 2.3, $c(\omega,x)$is relaxed and is

independent of x lateral position [6].

$$\left\{\partial_z^2 + \left[\frac{\omega^2}{c^2((\omega)} - k_x\right]\right\} P(\omega, k_x, z) = 0 \tag{2.3}$$

$$P(\omega, k_x, z + \Delta z) = e^{\pm j\sqrt{\frac{\omega^2}{c^2(\omega)} - k_x^2}\,\Delta z} P(\omega, k_x, z) \tag{2.4}$$

Solution of equation 2.3 is given by equation 2.4, it has two solutions i.e. up and down going waves downward extrapolation. In this equation, it is shown that how to get pressure $P(\omega, k_x, z + \Delta z)$ at next step $z + \Delta z$ from current pressure at z in the frequency-wavenumber domain [14].

Extrapolation operators are required which approximate this response accurately. From the equation it is clear that it is recursive process and repeated for all depth steps to get the final migrated image, where $j = \sqrt{-1}$. If velocity $c(\omega)$or bulk modulus $M(\omega)$is allowed to be complex, it will compensate for absorption [14], we can then write it as

$$\frac{\omega}{c(\omega)} = k_c - j\alpha_c.$$

2.3.2 Effect of Q parameter

According to the equation 2.5, the magnitude of wavenumber response must be close to one, not too large than one and not too less than one. Magnitude response above one will make the system unstable while less than one will attenuate the wavefields in the passband. In case of acoustic media the magnitude is almost

one in the passband and less than one in the evanescent region. While, in case of visco-acoustic media magnitude in passband is slightly above one to compensate for absorption and dispersion, this slight increase is according to the value of Q which corresponds to absorption. If the value of Q becomes too small then the magnitude response will lead the process to instability. For stable operation magnitude response should be thoroughly seen before applying to the prestack migration data set, to guarantee stability. In Figure 2.4, effect of Q is shown on the wavenumber magnitude response with different values of Q. For acoustic case $Q = \infty$, which means no absorption took place and there is no compensation. In extrapolation process phase is also important in the passband, while in evanescent region it is of no importance. Phase in the passband will reposition the seismic events accurately.

2.3.3 Wavenumber Response for Visco-Acoustic Extrapolation

In order to implement the design for compensating operator, ideal wavenumber response is required for visco-acoustic case. The ideal response incorporate the effect of attenuation compensation in terms of value of Q. In explicit depth $f-x$ migration the extrapolation process is a filtering process. The $f-x$ extrapolation filters (operators) are designed to compensate for dispersion and attenuation based on the absorption law of linear visco-acoustic wave equation given by equation 2.3. The objective here is to design the visco-acoustic $f-x$ extrapolators based on

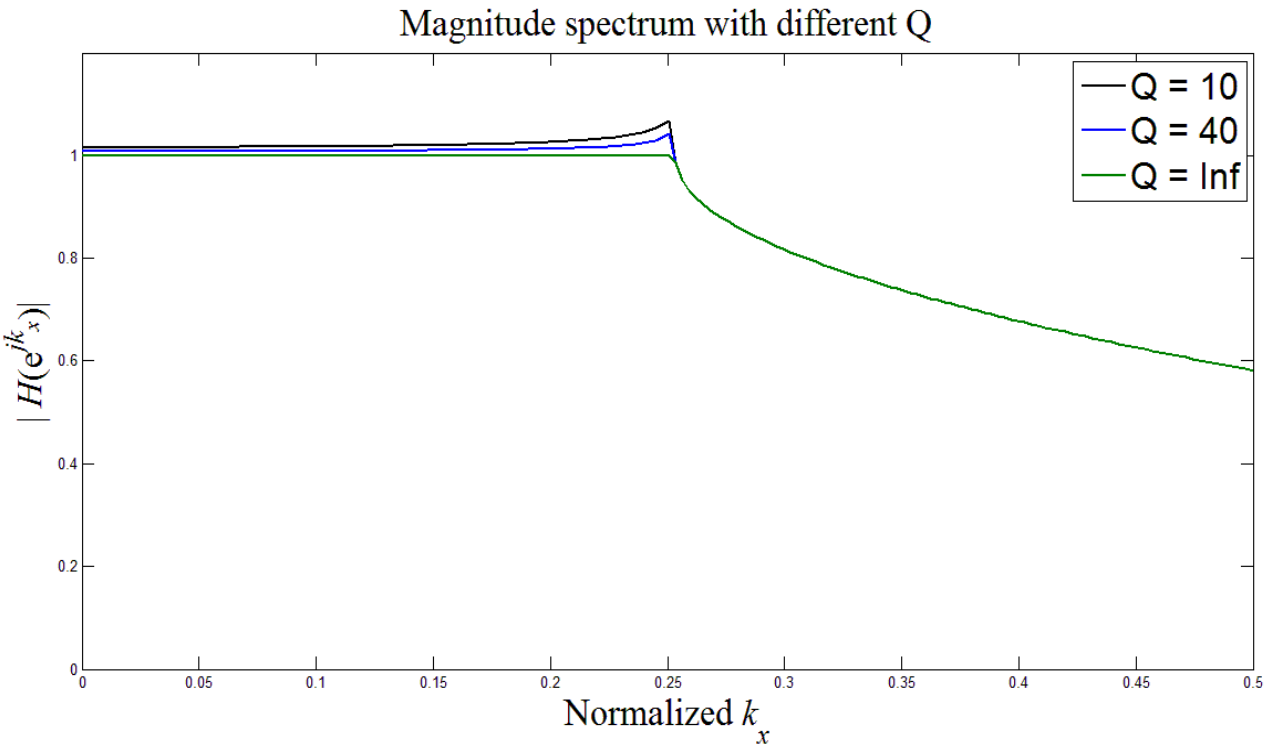

Figure 2.4: Effct of Q on the magnitude response.

the following 1-D normalized desired wavenumber response [15], that is given by:

$$H_d(k_x) \;=\; e^{jb\sqrt{(k_c - j\alpha_c)^2 - k_x^2}}, \tag{2.5}$$

where the term α_c is given as:

$$\alpha_c = \frac{k_c}{2Q}.$$

Note that b is ratio of the depth sampling to the horizontal lateral sampling i.e. $b = \frac{dz}{dx}$, k_c is the normalized cutoff, k_x is the normalized horizontal wavenumber and Q is the compensating parameter. There exists many ways to estimate the Q values. Here, we follow the work of [15] by which its value is square root of the velocity at each grid point of velocity model except for the water layer in which $Q = \infty$ (no attenuation). From equation 2.5, the cutoff is now a complex quantity, while in case of acoustic medium, the term $\alpha_c = 0$ because $Q = \infty$.

2.4 Sparse Filters

A general N length FIR filters that contain at most K nonzero coefficients (and $N - K$ zero coefficients) are called sparse FIR filters. Sparse FIR filters have been of interest to digital signal processing researchers since the mid-1990s. However, the design of sparse FIR digital filters has gained more interest after the introduction of compressive sensing [26, 27], a recent development in DSP offering the potential of high resolution acquisition of signals from relatively few measured samples under certain conditions. The few measured samples are typically below

the minimum number of samples based on Shannons sampling theorem [28]. Note that the only common factor between designing sparse FIR digital filters and the CS theory is the use of L_1-norm convex optimization methods, which are sparsity preserving.

2.5 Conclusions

In this chapter, a brief background for thesis work is discussed. An overview of seismic signal processing steps is highlighted. In the following chapters, to understand the designing process and apply the designs to the prestack depth migration of the Marmousi model data sets, prestack depth migration and visco-acoustic concepts are explained. Different types of migration details are briefly highlighted but the main focus is on explicit $f-x$ prestack depth migration. The visco-acoustics concepts are important for the thesis, for both data sets generation and migration of the data sets. In visco-acoustic case the main defining parameter is the value of Q, which is derived from the velocity model. Its effect is shortly shown in the figure, that how will it effect the magnitude wavenumber response of filter designs. The visco-acoustic wavenumber response is also highlighted, which is the main designing function in the thesis.

CHAPTER 3

VISCO-ACOUSTIC WAVEFIELD L_1-NORM FIR SPARSE FILTERS

3.1 Introduction

Most of the $f-x$ extrapolators designed for prestack and poststack migration consider the data to be acoustic in nature. In reality, seismic waves experience loss in energy when they propagate from the sources to the receivers. This loss in energy, if not compensated, reduces the data resolution. Depth migration is considered to be a physically more consistent and accurate domain to compensate and improve the resolution of the data at higher depths, as reported in [14] and [15]. Many authors used different approaches to design non-compensating acoustic medium wavefield extrapolators in the $f-x$ domain [6, 5, 8, 9, 7, 10, 11, 12,

13]. In this chapter, the $f-x$ extrapolation filters(operators) are designed to compensate for dispersion and attenuation based on the absorption law of linear visco-acoustic wave equation. The L_1-norm reported by [12] is used for the case of visco-acoustic medium to design compensating extrapolators that are sparse and non-sparse. Sparse coefficients require relatively low computational power because some coefficients are forced to be zero, with the expense of some allowed error in the design.

In the next section, the design of L_1-norm and its sparse version extrapolators is shown. To prove the concept of the designed operators, prestack depth migration is performed on the synthetic dataset of Marmousi model for both acoustic and visco-acoustic data. Finally, concluding remarks of the chapter are presented.

3.2 Design Algorithm for Sparse $f-x$ FIR Wavefield Operators for Visco-Acoustic Medium

The magnitude and phase responses of this extrapolator are even symmetric, which result in complex valued filter coefficients. Equation 2.5 can be approximated by:

$$H(e^{jk_x}) = \sum_{n=0}^{M} (2 - \delta[n]) h[n] \cos(nk_x)\,, \tag{3.1}$$

which is the wavenumber response of finite impulse response (FIR) filter with an odd length N and having a non-causal even symmetry [5, 9, 1, 12]. The filter coefficients $h[n] \in \mathbb{C}$ are complex valued, $M = (N-1)/2$ and $\delta[n]$ is unit sample

sequence.

3.2.1 Designing L_1-norm Visco-Acoustic Extrapolators

Let $\mathbf{h} = [[h[0]\ h[1]\ h[2]\ ...\ h[M]]^*$, which is a complex-valued vector representing the required extrapolation filter coefficients. Note that * denotes Hermitian conjugate, then the equation 3.1 can be written as:

$$H(e^{k_x}) = \mathbf{r}(k_x)\mathbf{h}, \tag{3.2}$$

where

$$\mathbf{r}(k_x) = [1 \quad \cos(k_x) \quad \cos(2k_x) \quad ... \quad \cos(Mk_x)], \tag{3.3}$$

and $\mathbf{R}$ as column of $\mathbf{r}(k_x)$ given as:

$$\mathbf{R} = \begin{bmatrix} \mathbf{r}(k_{x_1}) \\ \mathbf{r}(k_{x_2}) \\ . \\ . \\ \mathbf{r}(k_{x_L}) \end{bmatrix}. \tag{3.4}$$

Now, sample the wavenumber variable k_x into L points, k_{x_i}, where $i = 1, 2, 3, ..., L$. Then equation 3.2 can be written as:

$$H(e^{k_{x_i}}) = \mathbf{h}^*\mathbf{r}(k_{x_i}).$$

The design problem now turns into finding the points $H(e^k_{x_i})$ that match the desired wavenumber response (see equation 2.5) $H_d(k_{x_i})$ at k_{x_i} $i = 1, 2, 3, ..., L$. That is:

$$H(e^{k_{x_i}}) = H_d(k_{x_i}). \tag{3.5}$$

In a matrix form, for all points $(i = 1, 2, ..., L)$ along the wavenumber axis, equation 3.5 is given as:

$$\begin{bmatrix} H_d(k_{x_1}) \\ H_d(k_{x_2}) \\ . \\ . \\ H_d(k_{x_L}) \end{bmatrix} = \begin{bmatrix} \mathbf{r}(k_{x_1}) \\ \mathbf{r}(k_{x_2}) \\ . \\ . \\ \mathbf{r}(k_{x_L}) \end{bmatrix} \begin{bmatrix} h[0] \\ h[1] \\ . \\ . \\ h[M] \end{bmatrix}, \tag{3.6}$$

or

$$\mathbf{H}_d = \mathbf{R}\mathbf{h}, \tag{3.7}$$

where $\mathbf{H}_d$ is $L \times 1$, $\mathbf{R}$ is $L \times M$ dimension and $\mathbf{h}$ is a vector of length M. Now, to obtain sparse coefficients of the $f-x$ visco-acoustic extrapolation filters, we adopt the L_1-norm minimization. Following the work of [12], we aim to design N-length sparse and non-sparse $f-x$ visco-acoustic wavefield extrapolation filters by:

$$\min ||\mathbf{h}||_1$$

$$subject\ to\ ||\mathbf{H}_d - \mathbf{R}\mathbf{h}||_2 < \epsilon, \tag{3.8}$$

which is the L_1-norm minimization with quadratic constraint. Note that ϵ is a small positive number and is used for relaxing the quadratic constraints, which can be computed as [12]:

$$\epsilon = ||\mathbf{H}_d - \mathbf{R}\mathbf{h}^l||_2, \tag{3.9}$$

where $\mathbf{h}^l$ is the least square solution given as [29]:

$$\mathbf{h}^l = \mathbf{R}^*[\mathbf{R}\mathbf{R}^*]^{-1}\mathbf{H}_d. \tag{3.10}$$

3.3 Proposed L_1-norm Algorithm

The steps of the algorithm is as follow:

- Select the filter length N and cutoff k_c and Q value.
- Formulate the vector $\mathbf{H}_d$ using equation 2.5.
- Generate the matrix $\mathbf{R}$ using equation 3.4.
- Solve the L_1-norm minimization problem given in equation 3.8 to obtain the filter coefficients.
- Compute the threshold value and apply hard thresholding to find new $h[n]$ for sparse case based on [12].

3.3.1 Optimization Solution

The proposed L_1-norm convex optimization problem with quadratic constraints can be solved using method of log barrier [28] or disciplined convex programming [30], which can successfully solve L_1 convex problem with quadratic constraints. Once L_1-norm of $h[n]$ is minimized there is possibility that some coefficients has very small value (both real and imaginary parts), not necessarily zero because L_1-norm is sparsity preserving [31]. To obtain the sparse filter coefficients the method described by [12] is used.

3.3.2 Filter Designs

Figure 3.1 shows the designed extrapolation operators, Figure 3.2 shows spectral responses and Figure 3.3 shows errors for $k_c = 0.25$, $Q = 20$ with $N = 25$ and $N = 35$. In Figure 3.1, real and imaginary part of coefficients are shown. For the above parameters in the sparse version, out of $N = 25$, nine coefficients are set to zero, while for $N = 35$, ten coefficients are set to zero. The reduction in non-zero coefficients will reduce total number of flops for complex additions and multiplications, for further details on computational complexity calculation see [12]. Figures 3.2a and 3.2b show the magnitude and phase spectrum of the designed filter operators, respectively. Figures 3.3a and 3.3b show the magnitude and phase spectrum error, respectively. In case of non-compensated filters i.e. $Q = \infty$ (corresponds to water layers without attenuation) magnitude error is much less as compared to low value of Q. When the value of Q is reduced, the

error is slightly increased. That is why, in this section, smaller value of $Q = 20$ is used to show the accuracy of filters, for worst case scenario. Also, note the vertical scales for errors in the Figure 3.3a and 3.3b. The Marmousi model data, has a minimum value of $Q = 39$. In [15], the author stated that low values of Q, the designs become increasingly inaccurate. The designs, in this chapter, show how accurate they are even for low values of Q.

3.4 Prestack Imaging of the Marmousi Model Visco-Acoustic Data

The proposed L_1-norm $f - x$ extrapolation filters are tested on the Marmousi model seismic data. A synthetic data set is generated using Marmousi velocity model and derived Q model. The derived Q model has the same dimension as the velocity grid and is obtained by taking the square root of velocities at each grid point except for the water layer which corresponds to $Q = \infty$. High values of Q mean lower attenuation and vice-versa. So there is no attenuation in the water layer. The velocity ranges from 1500 m/s to 5500 m/s in the Marmousi model, so the corresponding range of Q is 39 to 75 for rest of the layers except water. The marmousi velocity model is shown in Figure 3.4 and the Q model is shown in the Figure 3.5.

For the both the acoustic and visco-acoustic shot gathers, finite difference modeling is used as reported by [32]. The visco-acoustic modeling require velocity

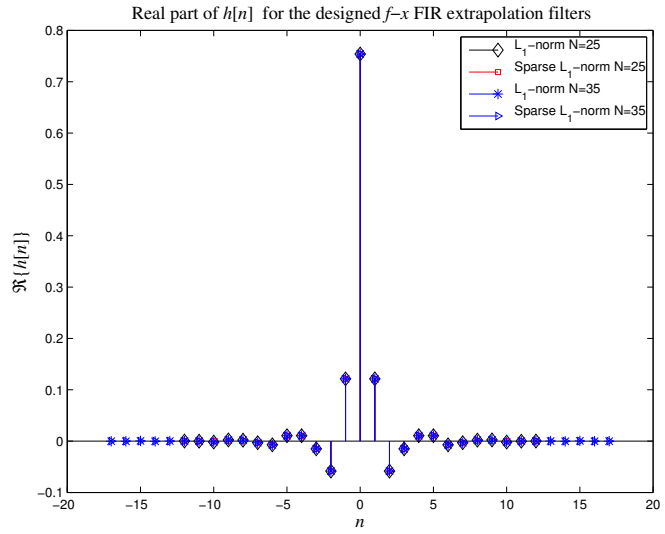

(a)

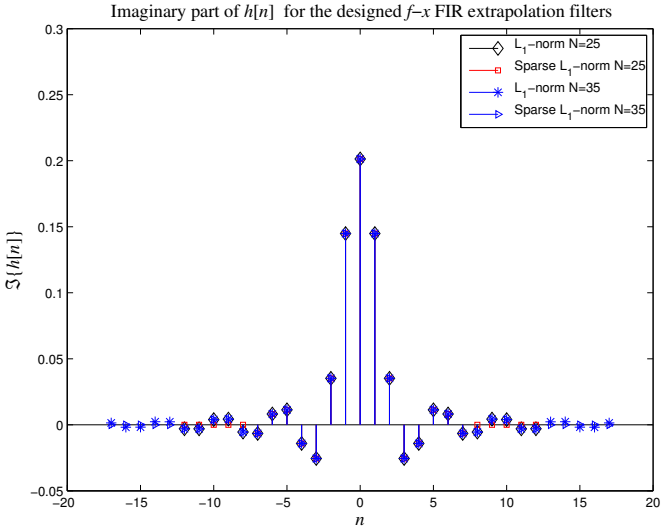

(b)

Figure 3.1: An example of compensating sparse and non-sparse $f-x$ extrapolation filters designed using the proposed L_1-norm method with $Q = 20$ and a normalized $k_c = 0.25$. (a) shows the real part and (b) shows the imaginary part of the designed filters' coefficients.

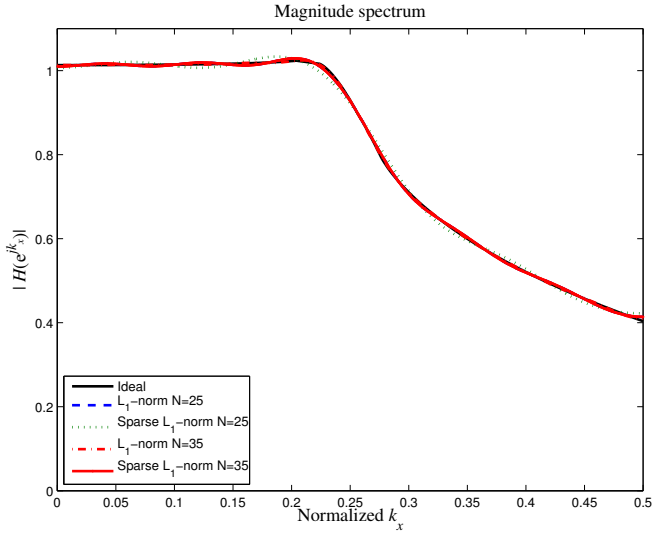

(a)

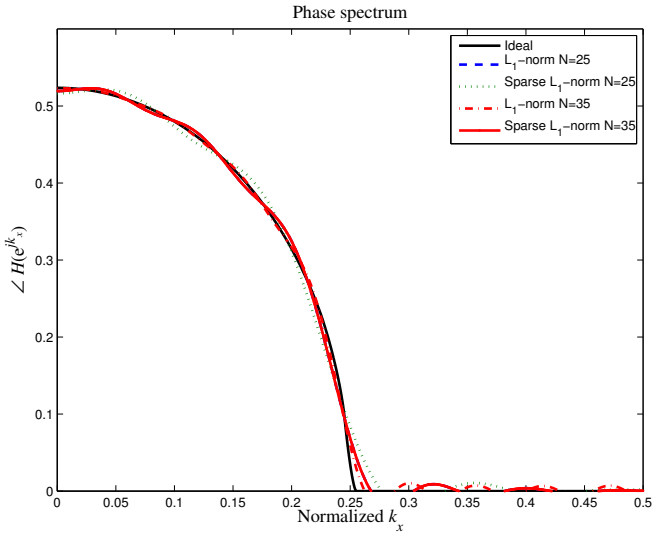

(b)

Figure 3.2: An example of compensating sparse and non-sparse $f-x$ extrapolation filters designed using the proposed L_1-norm method with $Q = 20$ and a normalized $k_c = 0.25$. (a) shows the magnitude spectrum and (b) shows the phase spectrum.

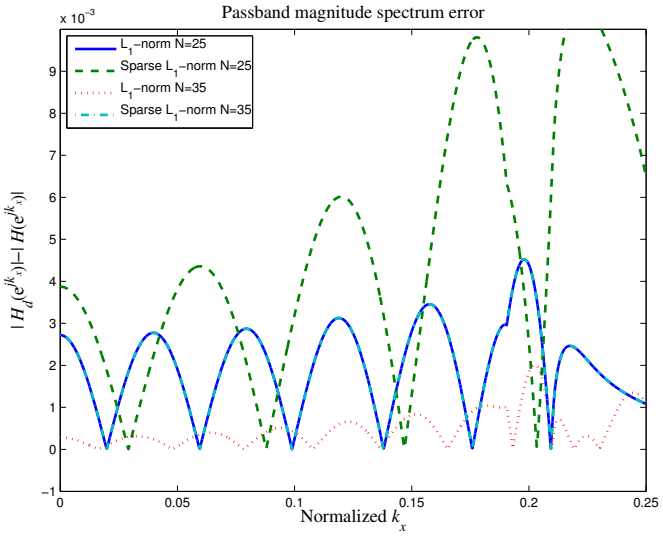

(a)

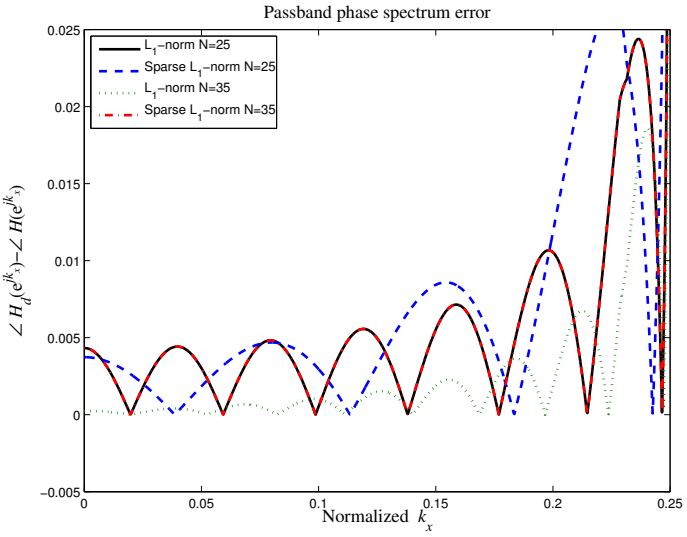

(b)

Figure 3.3: An example of compensating sparse and non-sparse $f-x$ extrapolation filters designed using the proposed L_1-norm method with $Q = 20$ and a normalized $k_c = 0.25$. (a) shows the passband magnitude response error and (b) shows phase response error.

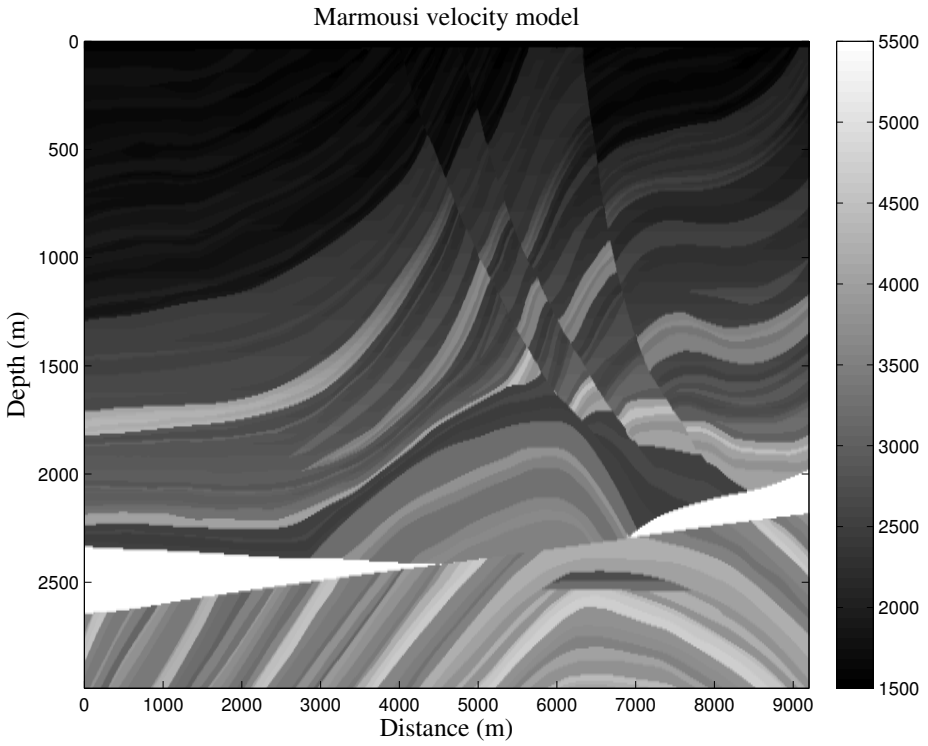

Figure 3.4: Marmousi velocity model.

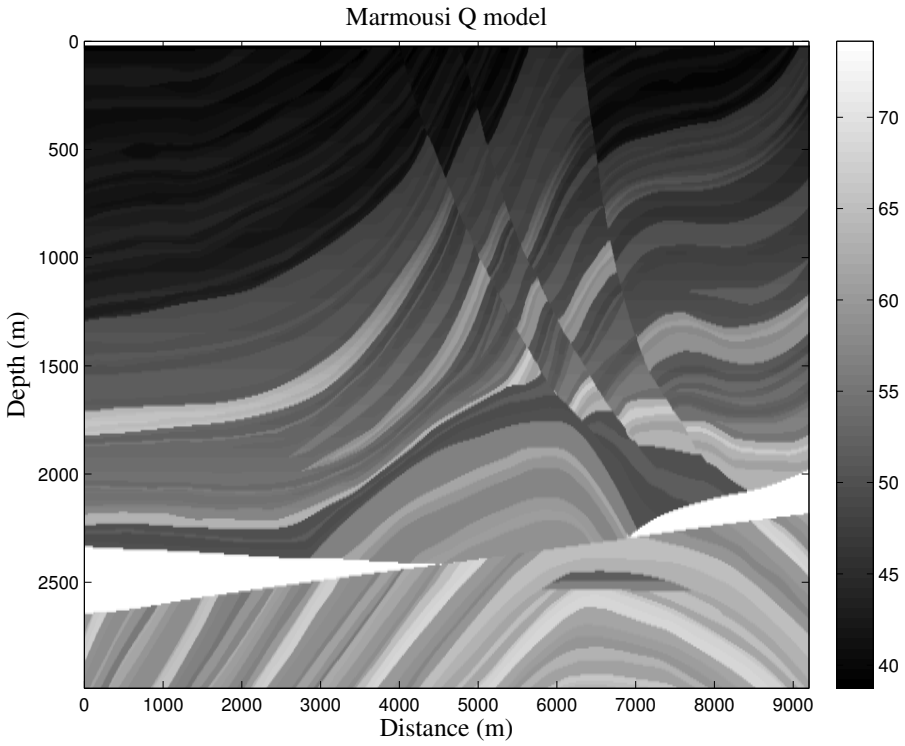

Figure 3.5: Marmousi Q model.

and Q model grids while the acoustic modeling require only the velocity model grid and density is kept constant for both the cases. In order to obtain stable shot gathers, the velocity and Q model grid spacings are kept 5 m for both dx and dz and time sampling is $dt = 0.4$ msec, the total recording time for each shot gather is 4 seconds.

Two datasets are generated, acoustic and visco-acoustic with the same parameters, parameters used here are the same as used in [15]. The shot interval is 50 m and the receiver interval is 25 m, maximum frequency of source wavelet is 45 Hz. In Figure 3.6a, the acoustic shot gather 100 is shown while Figure 3.6b shows the corresponding visco-acoustic shot gather. Both shot gathers are at source location 4950 m. From Figures 3.6a and 3.6b, it is clear that wave energy is attenuated when traveling in the visco-acoustic medium. For that reason, acoustic filters does not provide a good solution for extrapolation. Hence, compensated visco-acoustic filters are required to compensate for the attenuation in such a away that the migration remains practically stable, as the migration process is recursive.

Prestack depth migration is performed for three cases: (a) the acoustic operators migration on the acoustic data set, (b) the acoustic operators migration on the visco-acoustic data set and, finally, (c) the compensating visco-acoustic operators migration on the visco-acoustic data set. Note that, in all cases, the imaging condition used for the prestack depth migration is cross-correlation of both upward and downward fields for the compensated operators. All the cases are migrated with extrapolators of length $N = 25$ and $N = 35$ filter coefficients

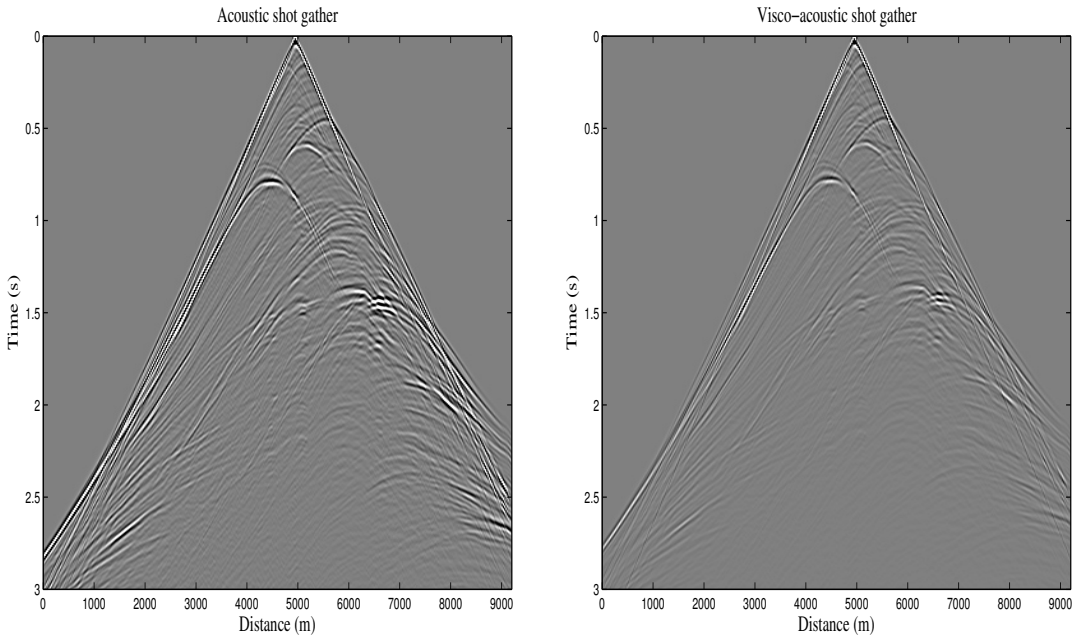

(a) (b)

Figure 3.6: Shot gather 100 at location 4950 m, (a) shows Acoustic data and (b) shows Visco-acoustic data.

for both the sparse and non-sparse designs.

Figures 3.7a-c show depth migrated sections using non-sparse filter and 3.8a-c show migrated sections using sparse filter coefficients with extrapolators of length $N = 25$. Figures 3.9a-c and 3.10a-c show the same migrated images but with $N = 35$. In Figures 3.11-3.14 the zoomed sections of area (lateral position, $3200 - 8000$ m; depth, $1950 - 2990$ m) are shown. Figures 3.11a-c show zoomed migrated sections of the non-sparse filters, while Figures 3.12a-c show migrated sections for the sparse case. Similarly, the Figures 3.13a-c and 3.14a-c show the same for $N = 35$. Clearly, the prestack depth migrated images using the compensating operators outperform those generated using non-compensating operators. For case of sparse filters with $N = 25$, the migrated images show that it has slightly salt and pepper noise near the end, while this effect is minimal for the image obtained using the sparse $f - x$ extrapolation filters with $N = 35$.

The envelope of the average value of traces at each depth level is plotted in the Figure 3.15. Again, it is clear that the compensating operators provide better seismic images than the non-compensating ones. At higher depth the resolution of the non-compensating operators is very low, on the other hand, both sparse and non-sparse compensating operators provide improved resolution. In Figure 3.15a, the sparse envelope is slightly deviating from non-sparse compensating operators while in Figure 3.15b, both sparse and non-sparse have more closer envelope.

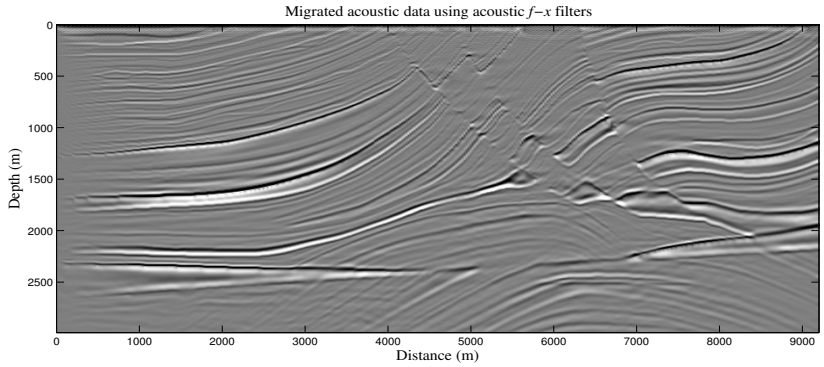

(a)

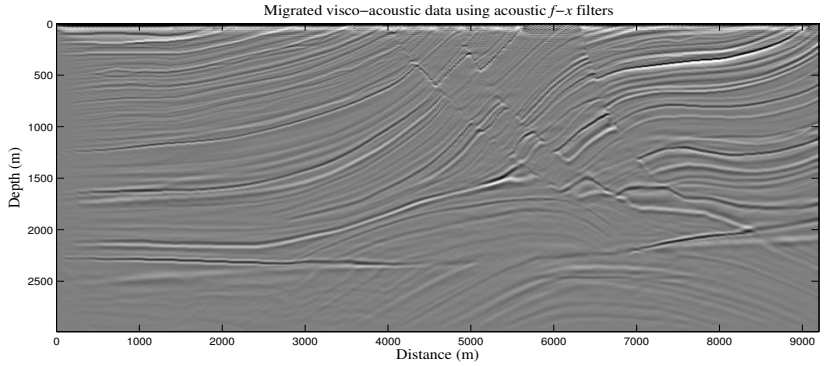

(b)

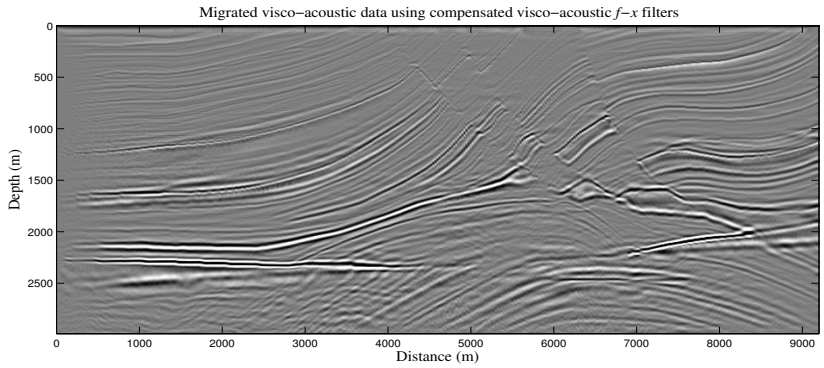

(c)

Figure 3.7: Migrated Marmousi images using the proposed non-sparse L_1-norm filters with $N = 25$. (a) and (b) show images obtained from applying acoustic (non-compensating) $f-x$ extrapolation filters to both acoustic and visco-acoustic data sets, respectively.(c) shows the resulting image after using the compensating $f - x$ extrapolation filters to the visco-acoustic data set.

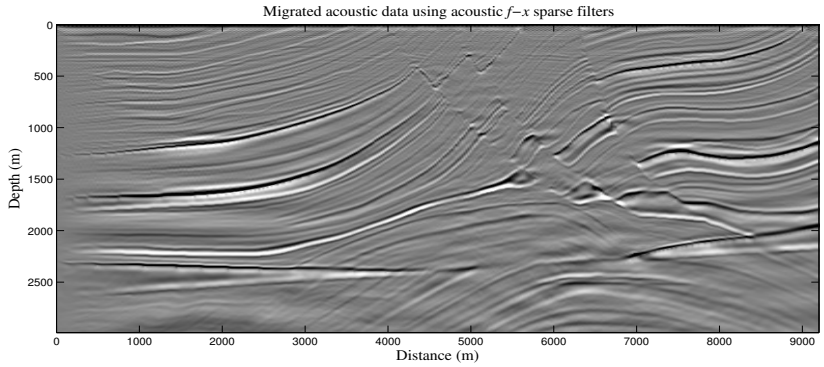

(a)

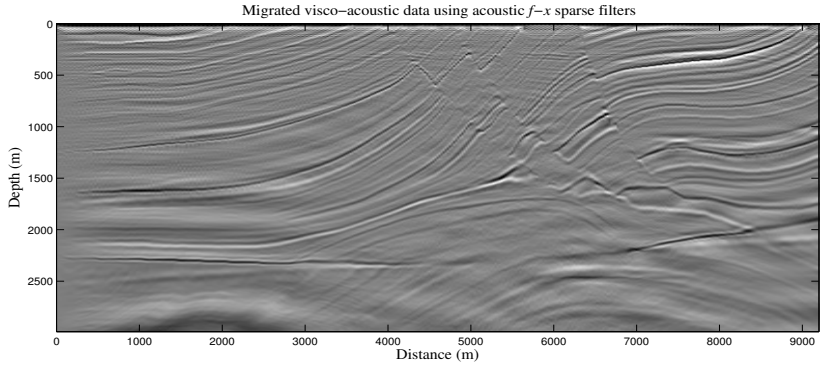

(b)

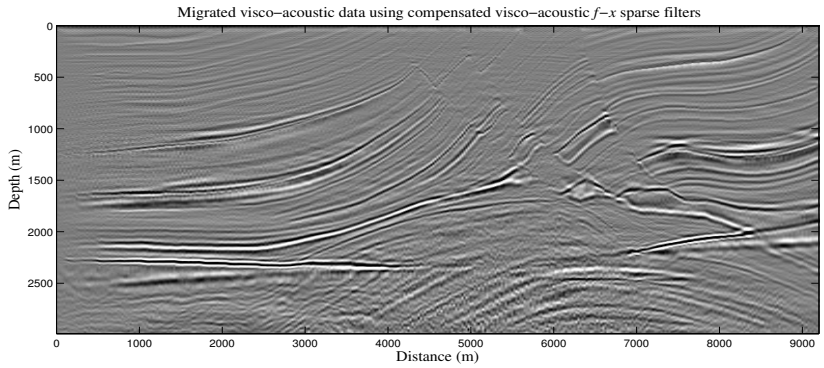

(c)

Figure 3.8: Migrated Marmousi images using the proposed sparse L_1-norm filters with $N = 25$. (a) and (b) show images obtained from applying acoustic (non-compensating) $f - x$ extrapolation filters to both acoustic and visco-acoustic data sets, respectively.(c) shows the resulting image after using the compensating $f - x$ extrapolation filters to the visco-acoustic data set.

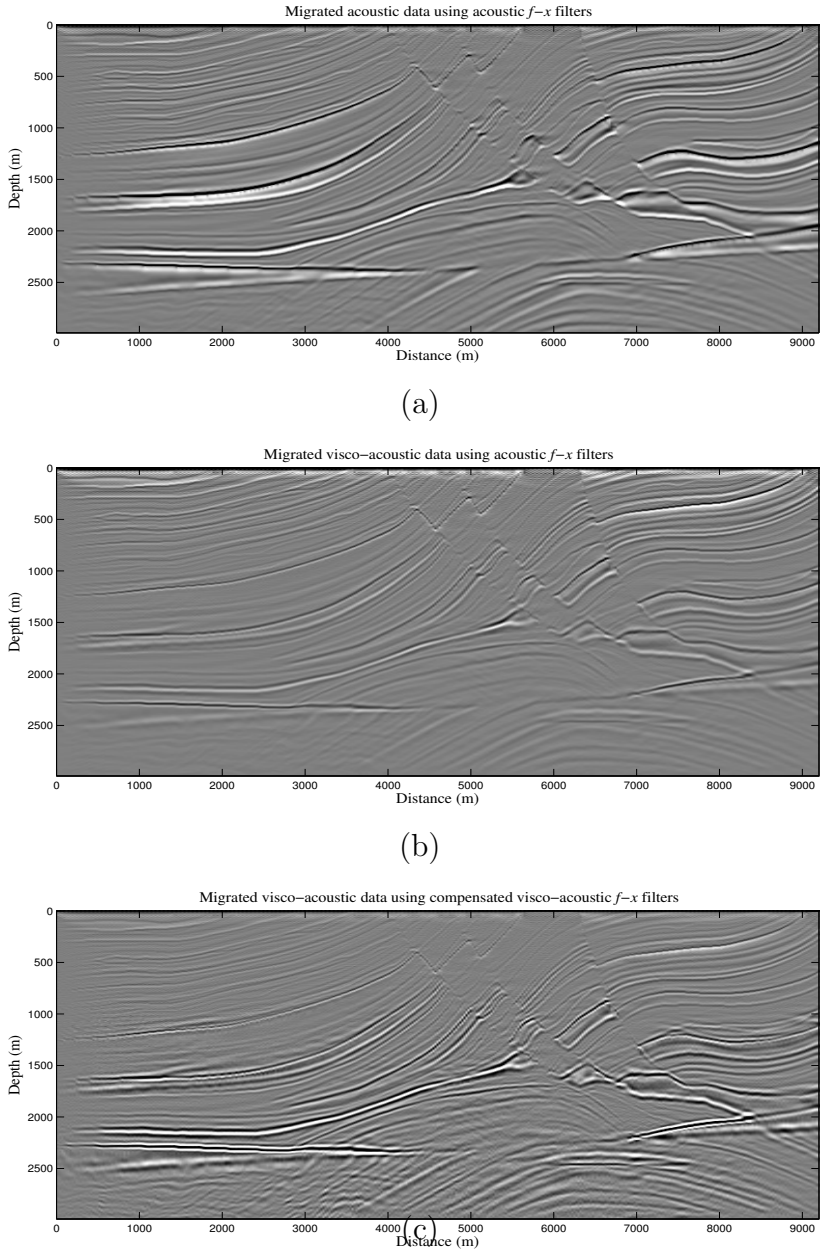

Figure 3.9: Migrated Marmousi images using the proposed non-sparse L_1-norm filters with $N = 35$. (a) and (b) show images obtained from applying acoustic (non-compensating) $f-x$ extrapolation filters to both acoustic and visco-acoustic data sets, respectively.(c) shows the resulting image after using the compensating $f - x$ extrapolation filters to the visco-acoustic data set.

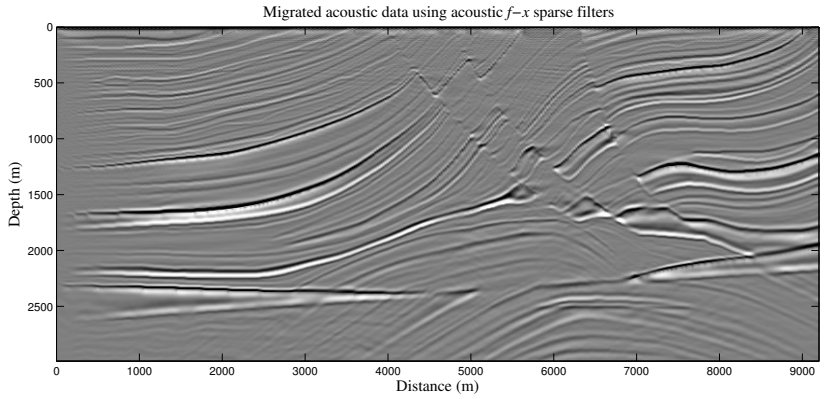

(a)

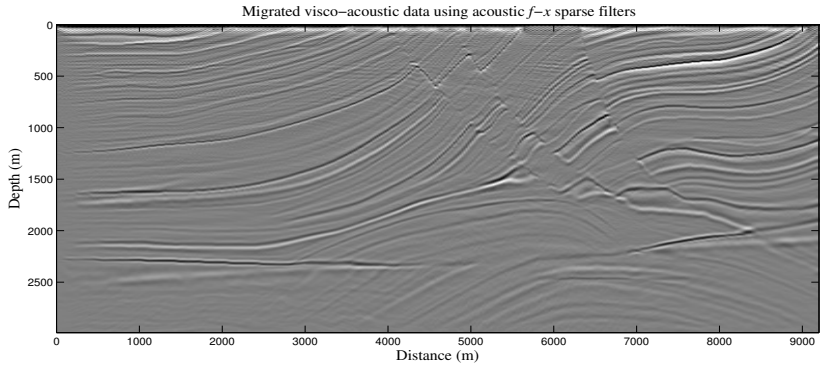

(b)

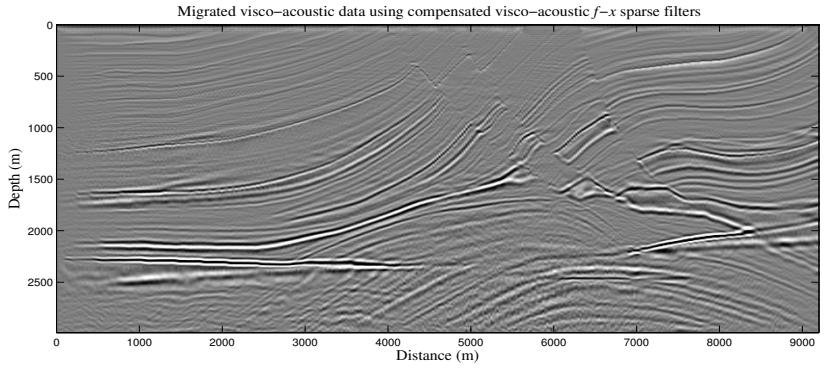

(c)

Figure 3.10: Migrated Marmousi images using the proposed sparse L_1-norm filters with $N = 35$. (a) and (b) show images obtained from applying acoustic (non-compensating) $f-x$ extrapolation filters to both acoustic and visco-acoustic data sets, respectively.(c) shows the resulting image after using the compensating $f-x$ extrapolation filters to the visco-acoustic data set.

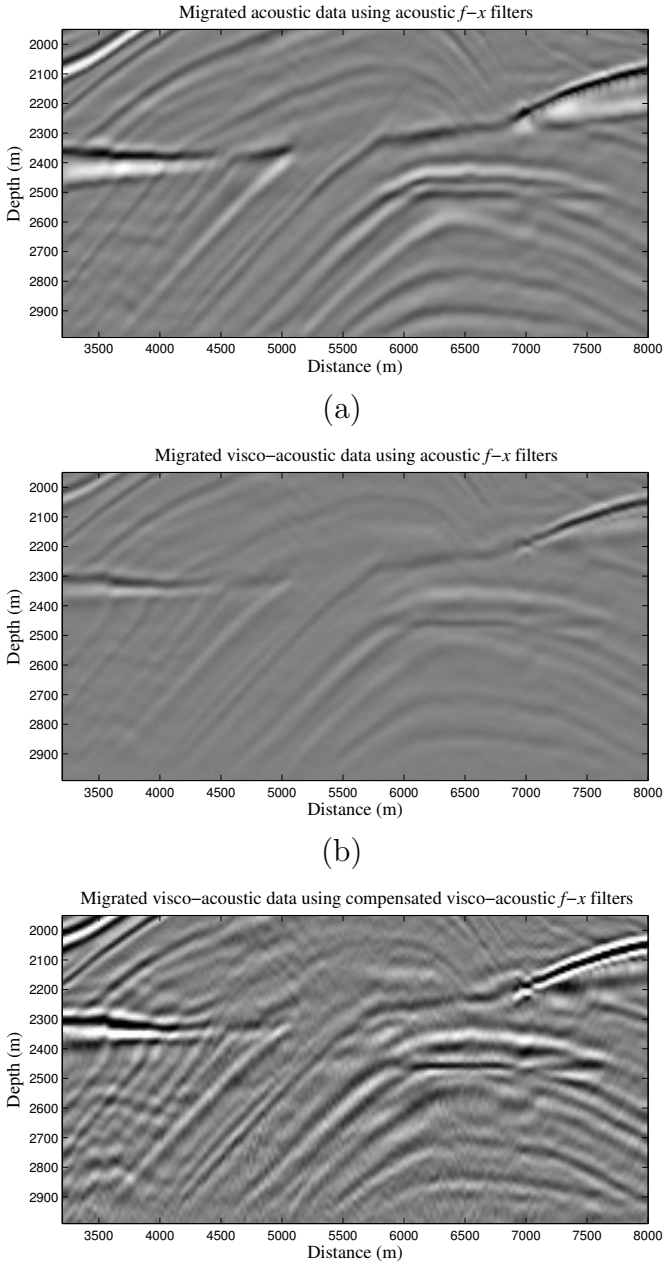

Figure 3.11: Zoom-in area of the migrated images using the proposed non-sparse L_1-norm ($N = 25$) (lateral position: $3200-8000$ m and depth: $1950-2990$ m). (a) and (b) show images obtained from applying acoustic (non-compensating) $f-x$ extrapolation filters to both acoustic and visco-acoustic data sets, respectively. (c) shows the resulting image after using compensating $f-x$ extrapolation filters to the visco-acoustic data set.

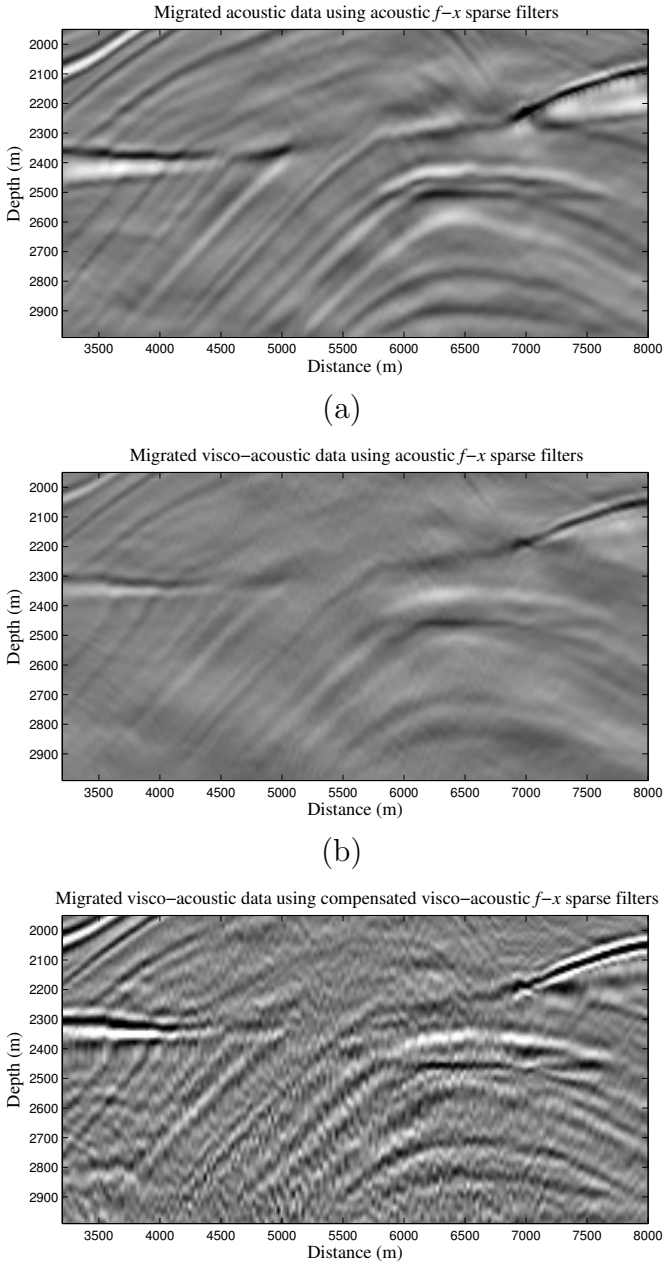

Figure 3.12: Zoom-in area of the migrated images using the proposed sparse L_1-norm ($N = 25$) (lateral position: $3200 - 8000$ m and depth: $1950 - 2990$ m). (a) and (b) show images obtained from applying acoustic (non-compensating) $f - x$ extrapolation filters to both acoustic and visco-acoustic data sets, respectively. (c) shows the resulting image after using the compensating $f - x$ extrapolation filters to the visco-acoustic data set.

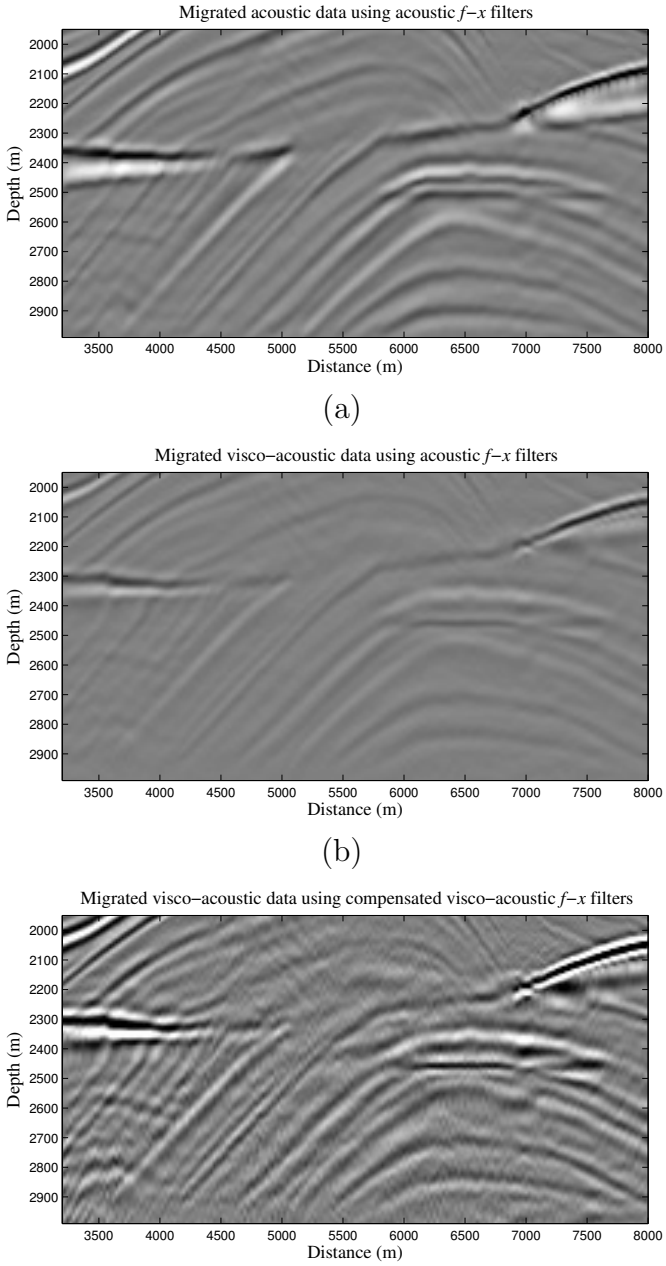

Figure 3.13: Zoom-in area of the migrated images using the proposed non-sparse L_1-norm ($N = 35$) (lateral position: $3200-8000$ m and depth: $1950-2990$ m). (a) and (b) show images obtained from applying acoustic (non-compensating) $f-x$ extrapolation filters to both acoustic and visco-acoustic data sets, respectively. (c) shows the resulting image after using compensating $f-x$ extrapolation filters to the visco-acoustic data set.

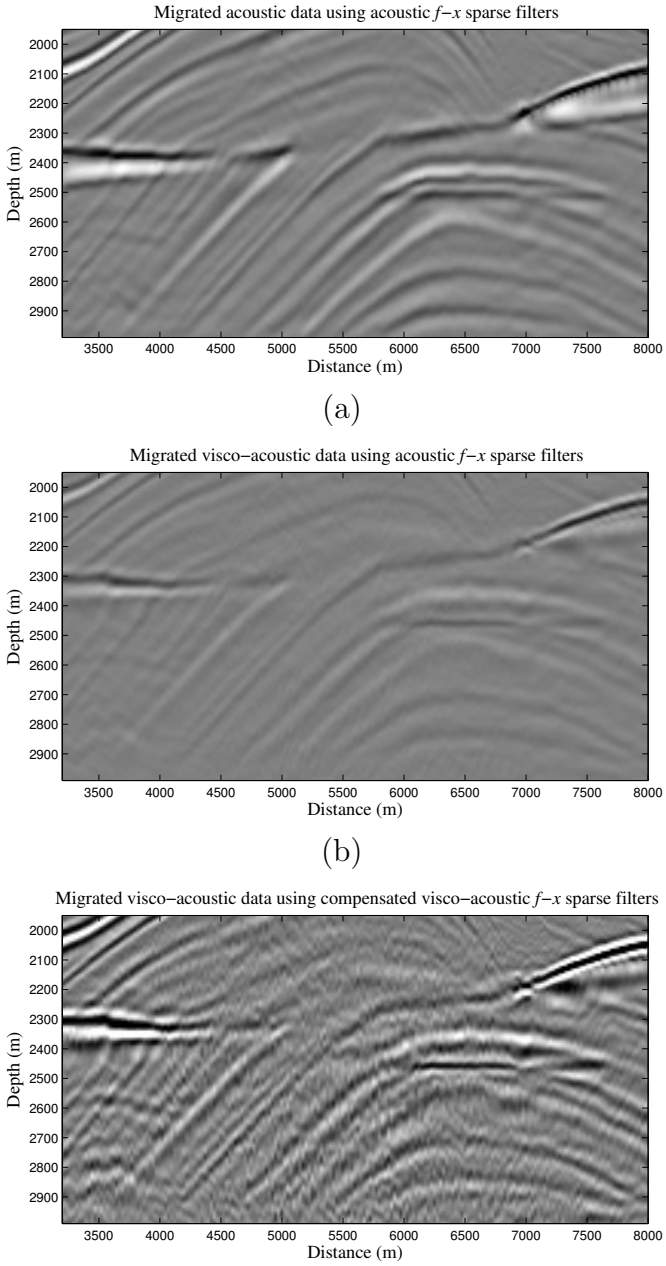

Figure 3.14: Zoom-in area of the migrated images using the proposed sparse L_1-norm ($N = 35$) (lateral position: $3200 - 8000$ m and depth: $1950 - 2990$ m). (a) and (b) show images obtained from applying acoustic (non-compensating) $f - x$ extrapolation filters to both acoustic and visco-acoustic data sets, respectively.(c) shows the resulting image after using the compensating $f - x$ extrapolation filters to the visco-acoustic data set.

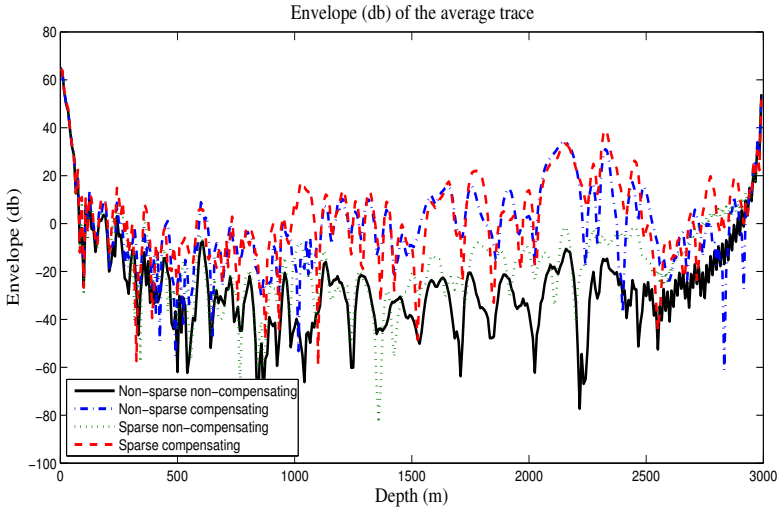

(a)

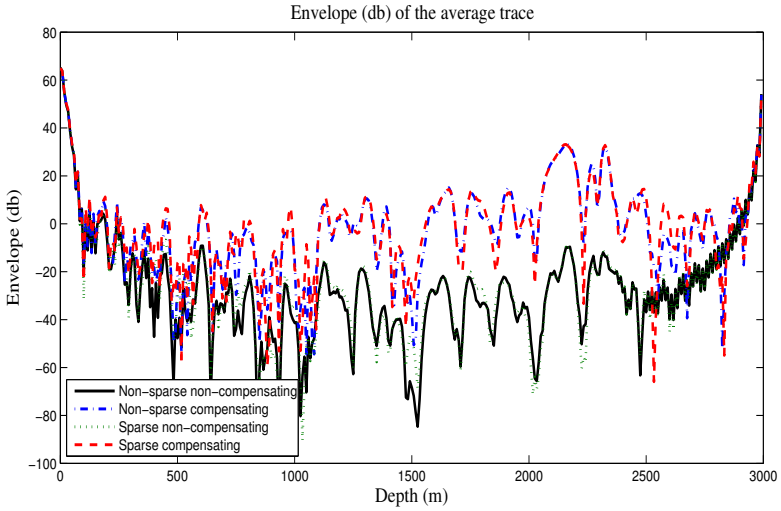

(b)

Figure 3.15: The envelopes of the average trace from images migrated using the proposed non-compensating and compensating sparse and non-sparse $f - x$ extrapolation filters with (a) $N = 25$ and (b) $N = 35$.

3.5 Discussion

At higher depths there are some small ringing events in the compensated $f-x$ filter migrated images. These ringing events were also discussed by [15]. If the maximum value of $k_c = \frac{fdx}{c_{min}}$ is less than Nyquist, these ringing events are reduced. To decrease this value either we decrease f_{max} of the source wavelet or dx but in practical scenario, it is difficult to vary these parameters. Lowering f_{max} decreases the resolution while lowering dx is like placing more receiver which is sometimes not feasible. In a practical scenario, probably, pre-processing of real data may reduce the high-frequency noise that is increasing these ringing events. In all cases, compensated operators will provide better results as compared to non-compensating operators for visco-acoustic data sets. As this prestack depth migration is recursive in nature and magnitude is slightly higher than one, this can make the process unstable. We have adopted a similar approach of smoothing reported by [10]. For the visco-acoustic case, the wavenumber response needs to be smoothed because there is slight discontinuity at the cutoff. For lower Q values this discontinuity increases in the magnitude of wavenumber response.

3.6 Computational Complexity

In terms of complex multiplications and additions, the total computational cost of the non-sparse explicit depth $f-x$ extrapolation for a given angular frequency

at one depth slice (for either up-going or down-going extrapolation) is:

$$COST_{+} = n_x \times (N-1), \tag{3.11}$$

for complex additions and

$$COST_{\times} = n_x \times \left(\frac{N+1}{2}\right), \tag{3.12}$$

for complex multiplications, where n_x is the total number of spatial samples (total number of traces per shot) and N is the filter length. Each complex addition requires two flops while each complex multiplication requires six flops [33]. To perform the prestack depth migration on the any benchmark model data set, the general formula for given angular frequency is given by:

$$TotalFlops_{+} = 2 \times nshots \times ndepth \times ntraces \times 2 \times (N-1), \tag{3.13}$$

where $TotalFlops_{+}$ is the total number of flops for complex additions. In case of multiplication the total flops (for given angular frequency) is given by:

$$TotalFlops_{\times} = 2 \times nshots \times ndepth \times ntraces \times 6 \times \left(\frac{N+1}{2}\right), \tag{3.14}$$

where $TotalFlops_{\times}$ is total number of flops for complex multiplications. Also, $nshots$ is total number of shot gathers, $ndepth$ is total number of depths, $ntraces$ is total number of traces per shot gather. The factor 2 in both the calculation is

because of down-going and up-going extrapolation in the prestack depth migration, same process is repeated twice with corresponding filter coefficients.

Now in sparse case, the number of non-zero coefficients are K so the equation becomes:

$$SCOST_{+} = n_x \times (K-1), \tag{3.15}$$

for complex additions and

$$SCOST_{\times} = n_x \times \left(\frac{K+1}{2}\right), \tag{3.16}$$

for complex multiplications. And the total flops equations for addition and multiplication are given by:

$$STotalFlops_{+} = 2 \times nshots \times ndepth \times ntraces \times 2 \times (K-1), \tag{3.17}$$

and

$$STotalFlops_{\times} = 2 \times nshots \times ndepth \times ntraces \times 6 \times \left(\frac{K+1}{2}\right). \tag{3.18}$$

Here, in case of Marmousi model data, the total shot gathers are $nshot = 209$ shots, each shot has $ntraces = 417$ traces, total number of depths are $ndepth = 362$ depths. For instance, the cost of prestack depth migration for given angular frequency using the explicit depth non-sparse $f-x$ wavefield extrapolation filters of length $N = 35$ will be equal to $2 \times 209 \times 362 \times 417 \times 2 \times 34 = 4,290,716,496$

flops for the complex additions and $2 \times 209 \times 362 \times 417 \times 6 \times 18 = 6,814,667,376$ flops for the complex multiplications; both are per a given angular frequency. Of course, this takes into account the symmetry of the filter coefficients. Similarly, for sparse case of $N = 35$ (if we assume on average 10 zeros) with $K = 25$, the complexity is $2 \times 209 \times 362 \times 417 \times 2 \times 24 = 3,028,741,056$ flops for the complex additions and $2 \times 209 \times 362 \times 417 \times 6 \times 13 = 4,921,704,216$ flops for the complex multiplications; both are per a given angular frequency. In Table 3.1 the comparison of computational cost for sparse and non-sparse is shown. For non-sparse N represents the filter length. While in case of non-sparse some coefficients are zero, so K represents the number of non-zero filter coefficients. The $N = 25$ and 35 are for non-sparse computational complexity. For sparse filters, $K = 17$ means $N = 25$ assuming eight zeros and $K = 25$ means $N = 35$ assuming ten zeros. The computational complexity of $N = 25$ non-sparse is the same as $N = 35$ (or $K = 25$) sparse case.

Filter length	$\times's$ flops	Savings in $\times's$	$+'s$ flops	Savings in $+'s$
$N = 25$	65052	-	40032	-
$K = 17$	45036	30.77 %	26688	33.33 %
$N = 35$	90072	-	56712	-
$K = 25$	65052	27.28 %	40032	29.41 %

Table 3.1: Comparison of Computation Cost (Flops for additions and multiplications) for each angular frequency at each depth slice (single shot gather) for Marmousi model.

In Table 3.2 the number of non-zero filter coefficients are shown for both sparse and non-sparse $f - x$ extrapolators. It shows details for one filter bank of 7377 filters. Decrease in the number of non-zero filter coefficients result in increasing the computational performance.

N	Non-sparse	Sparse	Reduction
25	184425	122218	33.73 %
35	258195	185732	28.83 %

Table 3.2: Number of non-zero filter coefficients.

3.7 Conclusions

We proposed the L_1-norm to design visco-acoustic explicit depth $f-x$ sparse and non-sparse wavefield extrapolators. Acoustic designs can easily be transformed to compensated visco-acoustic designs by adding the effect of Q value and followed by smoothing of the response. The designed filters resulted in practically stable prestack seismic images of the challenging Marmousi data set. The compensating filters enhanced the resolution as function of depth by applying to prestack depth migration. From the Marmousi images, it is evident that the sparse $f-x$ filters results in some ringings effects at the higher depth, although they can save some convolution operations as compared to the non-sparse ones.

CHAPTER 4

VISCO-ACOUSTIC WAVEFIELD WEIGHTED L_1-ERROR FIR FILTERS

4.1 Introducation

In this chapter, the method of weighted L_1-error is used to design the required compensating operators. In chapter 3, the L_1-norm of the operators is minimized, subject to the quadratic constraint of the error. Here, the required operators are design which reduce the L_1-error between the ideal and the designed wavenumber response. In this case, the objective function is minimization of the error. If same number of coefficients are used, the L_1-error will perform better because here the optimization problem focus on minimizing the error instead of minimizing the coefficients, which was the case in the L_1-norm minimization. The error, here, is

assumed to be sparse. In explicit $f-x$ extrapolation, the error minimization of passband is more important than the evanescent region. Because of the recursive nature of algorithm, the wavenumber in the evanescent region decays after few iterations. The passband should be given more priority, ideally in the passband, the magnitude should remain constant and phase should be hyperbolic. Hence, we also weight the error, the weighting term in the designing problem solve this problem by giving more weights to the passband as compared to the evanescent region.

4.2 Designing Weighted L_1-Error FIR Filters

Formulating the weighted L_1-error approximation for visco-acoustic wave equation is discussed in this section. Consider the desired 1-D visco-acoustic extrapolation filter's wavenumber response in the equation 2.5, the magnitude and phase response of these extrapolators are even symmetric, because of even symmetry filter coefficients are complex valued. In this chapter, the minimization problem is treated differently. Rather than finding the L_1-norm of filter coefficients, the L_1-norm of error is minimized. Now in this case the error is sparse. Let $\mathbf{h} = [[h[0]\ h[1]\ h[2]\ ...\ h[M]]^*$, which is a complex-valued vector representing the required extrapolation filter coefficients. Note that * denotes Hermitian conjugate, then the equation 3.1 can be written as:

$$H(e^{k_x}) = \mathbf{r}(k_x)\mathbf{h}, \tag{4.1}$$

where

$$\mathbf{r}(k_x) = [1 \quad \cos(k_x) \quad \cos(2k_x) \quad ... \quad \cos(Mk_x)], \tag{4.2}$$

and $\mathbf{R}$ as column of $\mathbf{r}(k_x)$ given as:

$$\mathbf{R} = \begin{bmatrix} \mathbf{r}(k_{x_1}) \\ \mathbf{r}(k_{x_2}) \\ . \\ . \\ \mathbf{r}(k_{x_L}) \end{bmatrix}. \tag{4.3}$$

Now, sample the wavenumber variable k_x into L points, k_{x_i}, where $i = 1, 2, 3, ..., L$. Then equation 4.1 can be written as:

$$H(e^{k_{x_i}}) = \mathbf{h}^* \mathbf{r}(k_{x_i}).$$

The design problem now turns into finding the points $H(e^k_{x_i})$ that match the desired wavenumber response (see equation 2.5) $H_d(k_{x_i})$ at k_{x_i} $i = 1, 2, 3, ..., L$. That is:

$$H(e^{k_{x_i}}) = H_d(k_{x_i}). \tag{4.4}$$

In a matrix form, for all points ($i = 1, 2, ..., L$) along the wavenumber axis, equation 4.4 is given as:

$$\begin{bmatrix} H_d(k_{x_1}) \\ H_d(k_{x_2}) \\ . \\ . \\ H_d(k_{x_L}) \end{bmatrix} = \begin{bmatrix} \mathbf{r}(k_{x_1}) \\ \mathbf{r}(k_{x_2}) \\ . \\ . \\ \mathbf{r}(k_{x_L}) \end{bmatrix} \begin{bmatrix} h[0] \\ h[1] \\ . \\ . \\ h[M] \end{bmatrix}, \tag{4.5}$$

or

$$\mathbf{H}_d = \mathbf{R}\mathbf{h}, \tag{4.6}$$

where $\mathbf{H}_d$ is $L \times 1$, $\mathbf{R}$ is $L \times M$ dimension and $\mathbf{h}$ is a vector of length M. Now the objective function here is to find the filter coefficients which minimize the L_1-norm of the error between the ideal desired response and the designed response which is given as:

$$\min_h \ \|\mathbf{H}_d - \mathbf{R}\mathbf{h}\|_1, \tag{4.7}$$

where $\mathbf{H}_d$ is the ideal desired wavenumber response given by equation 2.5 for visco-acoustic case. In fact L_1-error minimization technique try to obtain the sparse difference. The approximating error via L_1 can result in a few large significant values. To address this issue, the performance of L_1-norm can be improved by emphasizing more weights on passband wavenumber, when compared to the evanescent region so that equation 4.7 can be written as:

$$\min_h \ \|\mathbf{W}(\mathbf{H}_d - \mathbf{R}\mathbf{h})\|_1, \tag{4.8}$$

where

$$\mathbf{W} = \begin{bmatrix} W_p & 0 \\ 0 & W_s \end{bmatrix}, \tag{4.9}$$

is the diagonal weighting matrix. the weights of the pass band is given by W_p and evanescent region by W_s. These weights are chosen in such away to give more priority to passband which is more important as compared to evanescent region of the wavenumber response. In later sections, it will be shown that weighted version of extrapolators perform better than its non-weighting counterpart. Non-weighting designs can be considered as special case of weighting, if the weight matrix is considered to be identity matrix.

4.3 Weighted L_1-error Algorithm

The steps of the proposed weighted L_1-error algorithm is as follow:

- Select the filter length N and cutoff k_c and Q value.
- Formulate the vector $\mathbf{H}_d$ using equation 2.5.
- Generate the matrices $\mathbf{R}$ and $\mathbf{W}$ using equations 4.3 and 4.9.
- Solve the weighted L_1-error minimization problem given in equation 4.8 to obtain the filter coefficients.

The proposed L_1-error minimization problems given by equations 4.7 and 4.8 can be solved using CVX optimization toolbox [30].

4.4 Simulation Results

The parameters used for simulation purpose here are the same as used in chapter 3, i.e, $k_c = 0.25$, $Q = 20$ with $N = 25$. Figures 4.1a and 4.1b show the magnitude and phase spectrum of the designed filter operators, respectively. Figures 4.2a and 4.2b show the magnitude and phase spectrum error, respectively. The designs with weighting, show how accurate they are even for low values of Q.

The envelope of the average value of traces at each depth level is plotted in the Figure 4.7. Again, it is clear that the compensating operators provide better seismic images than the non-compensating ones. At higher depth the resolution of the non-compensating operators is very low, on the other hand, both weighted and non-weighted compensating operators provide improved resolution.

4.5 Prestack Imaging of the Marmousi Model Visco-Acoustic Data

The datasets used for acoustic and visco-acoustic cases are the same as in chapter 3. Prestack depth migration is performed for three cases: (a) the acoustic operators migration on the acoustic data set, (b) the acoustic operators migration on the visco-acoustic data set and, finally, (c) the compensating visco-acoustic operators migration on the visco-acoustic data set. Note that, in all cases, the imaging condition used for the prestack depth migration is cross-correlation of both upward and downward fields for the compensated operators. All the cases

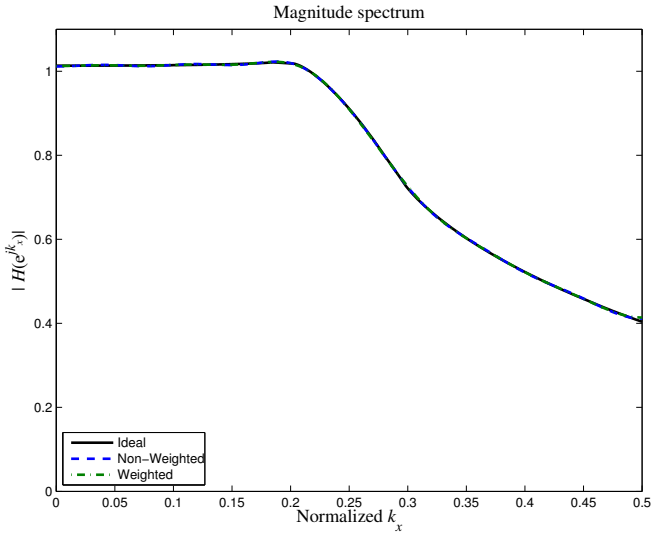

(a)

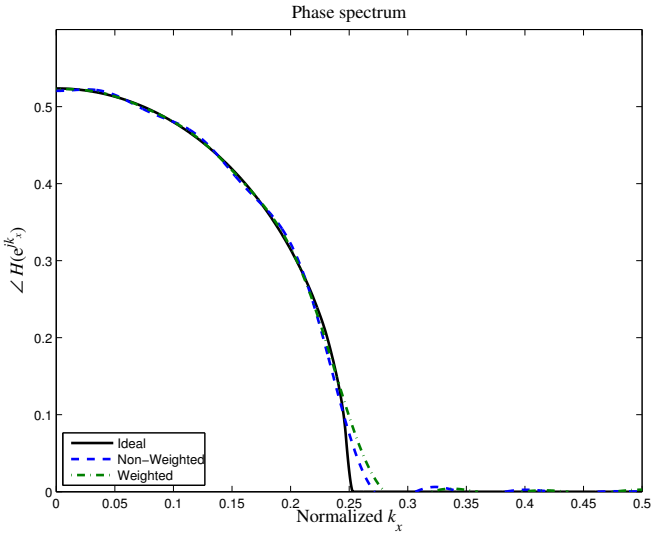

(b)

Figure 4.1: An example of compensating weighted and non-weighted $f - x$ extrapolation filters designed using the proposed L_1-error method with $Q = 20$ and a normalized $k_c = 0.25$. (a) shows the magnitude spectrum and (b) shows the phase spectrum.

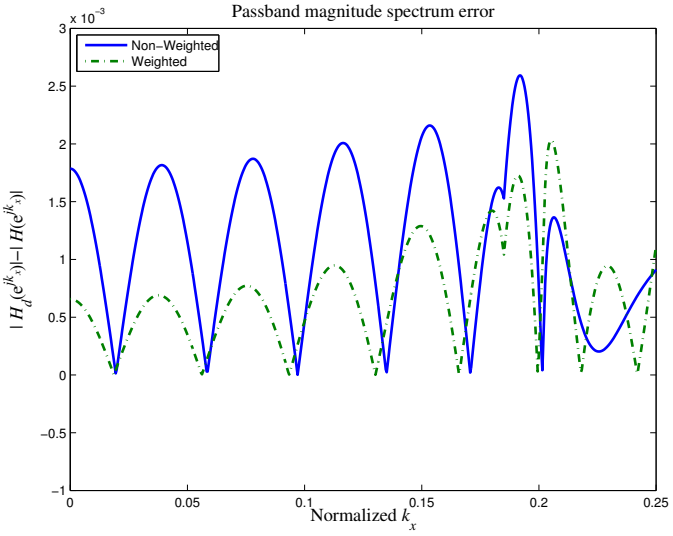

(a)

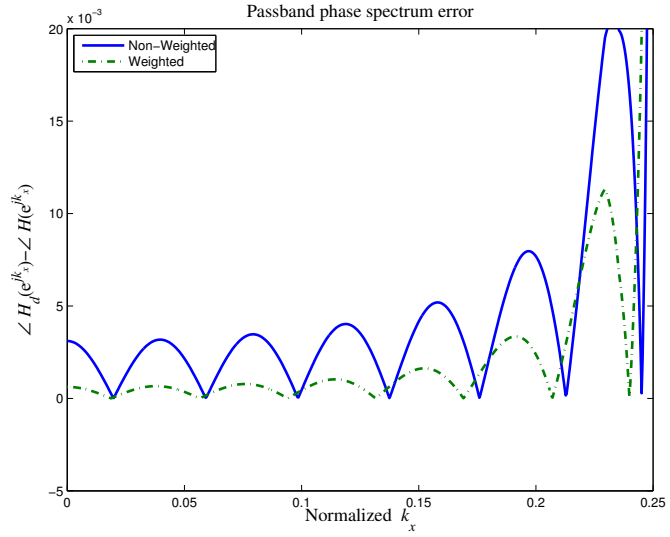

(b)

Figure 4.2: An example of compensating weighted and non-weighted $f - x$ extrapolation filters designed using the proposed L_1-error method with $Q = 20$ and a normalized $k_c = 0.25$. (a) shows the passband magnitude response error and (b) shows phase response error.

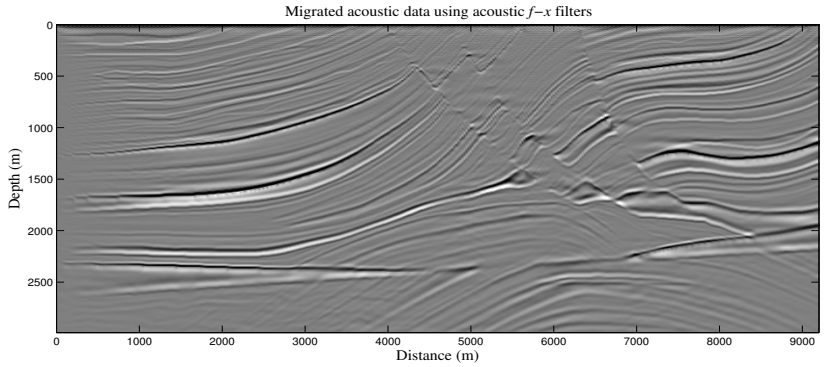

(a)

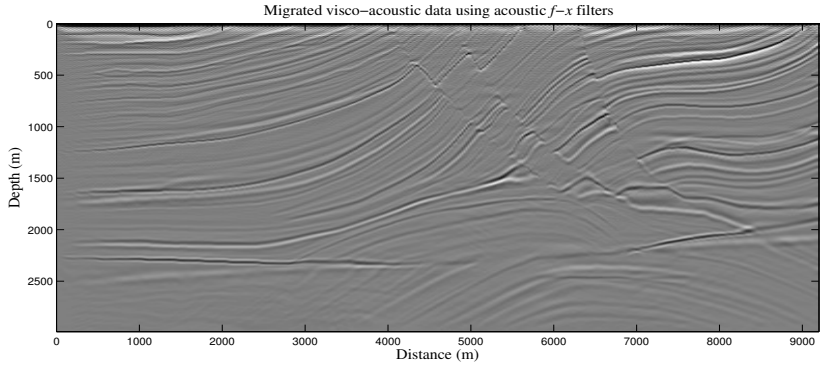

(b)

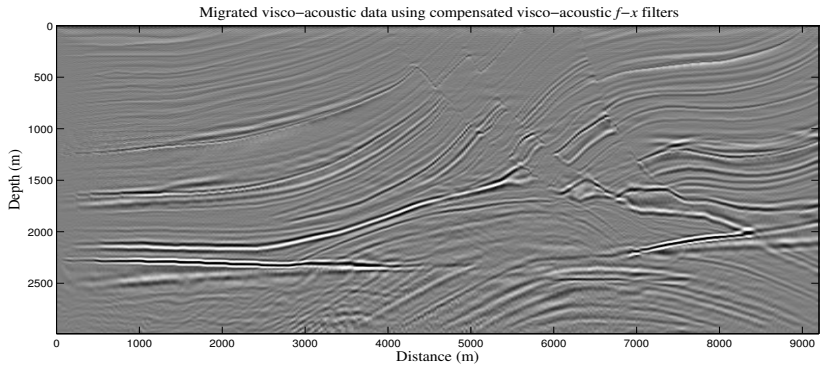

(c)

Figure 4.3: Migrated Marmousi images using the proposed non-weighted L_1-error filters with $N = 25$. (a) and (b) show images obtained from applying acoustic (non-compensating) $f-x$ extrapolation filters to both acoustic and visco-acoustic data sets, respectively.(c) shows the resulting image after using the compensating $f - x$ extrapolation filters to the visco-acoustic data set.

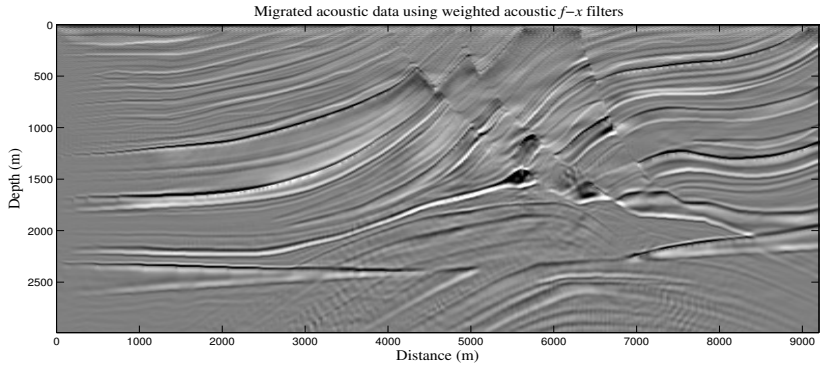

(a)

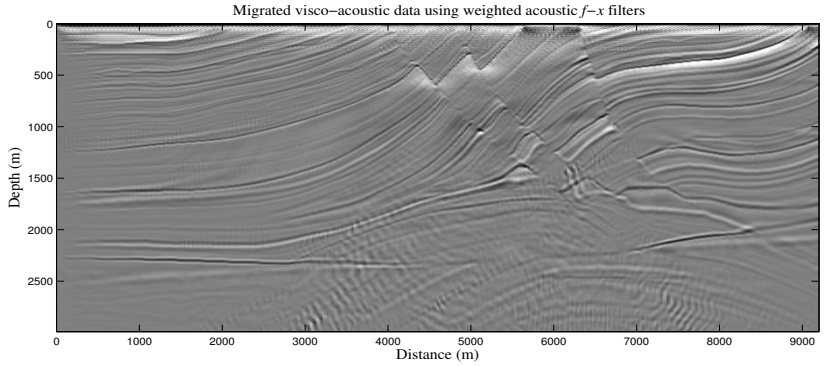

(b)

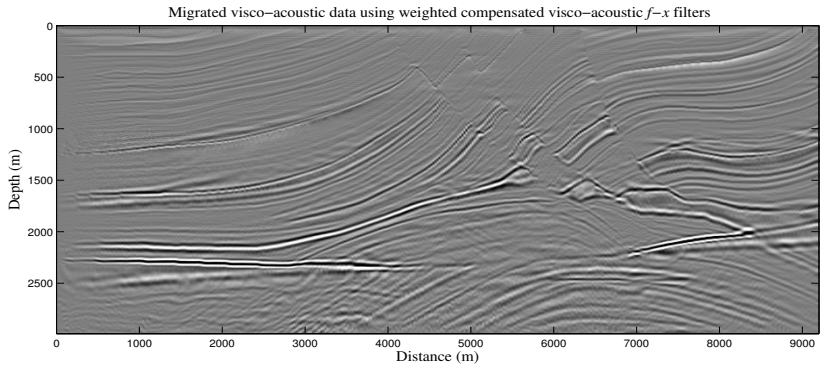

(c)

Figure 4.4: Migrated Marmousi images using the proposed weighted L_1-error filters with $N = 25$. (a) and (b) show images obtained from applying acoustic (non-compensating) $f-x$ extrapolation filters to both acoustic and visco-acoustic data sets, respectively.(c) shows the resulting image after using the compensating $f - x$ extrapolation filters to the visco-acoustic data set.

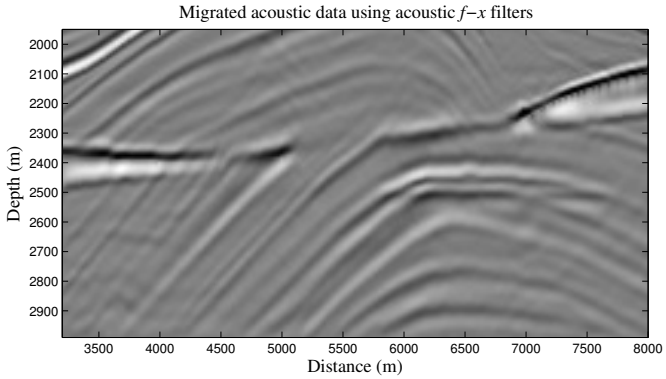

(a)

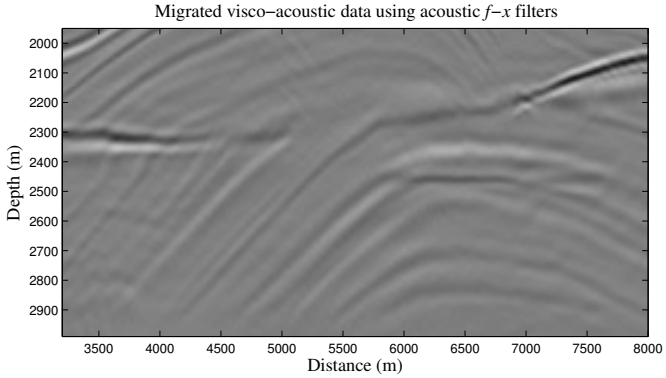

(b)

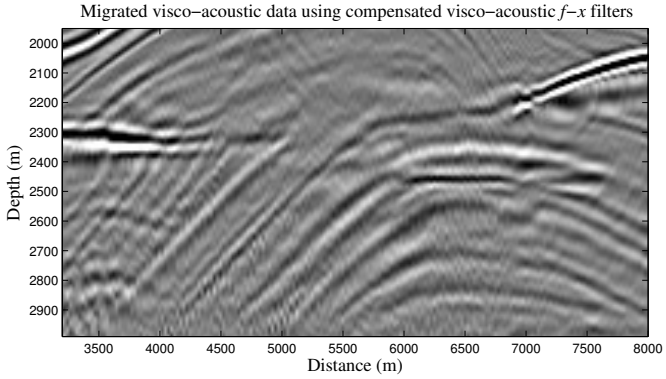

(c)

Figure 4.5: Zoom-in area of the migrated images using the proposed non-weighted L_1-error ($N = 25$) (lateral position: $3200-8000$ m and depth: $1950-2990$ m). (a) and (b) show images obtained from applying acoustic (non-compensating) $f-x$ extrapolation filters to both acoustic and visco-acoustic data sets, respectively. (c) shows the resulting image after using compensating $f-x$ extrapolation filters to the visco-acoustic data set.

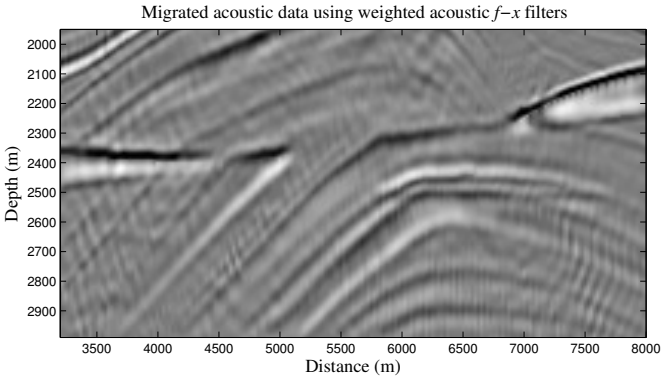

(a)

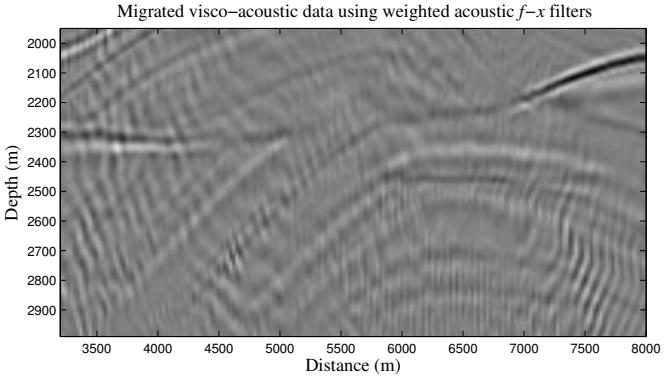

(b)

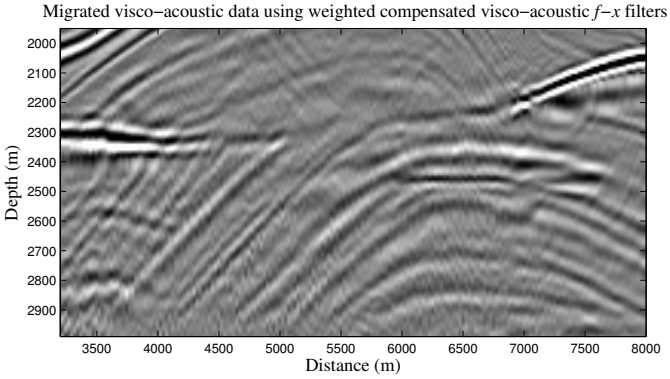

(c)

Figure 4.6: Zoom-in area of the migrated images using the proposed weighted L_1-error ($N = 25$) (lateral position: $3200 - 8000$ m and depth: $1950 - 2990$ m). (a) and (b) show images obtained from applying acoustic (non-compensating) $f - x$ extrapolation filters to both acoustic and visco-acoustic data sets, respectively. (c) shows the resulting image after using compensating $f - x$ extrapolation filters to the visco-acoustic data set.

are migrated with extrapolators of length $N = 25$ filter coefficients for both the weighted and non-weighted designs.

Figures 4.3a-c show depth migrated sections using non-weighted filter and 4.4a-c show migrated sections using weighted filter coefficients with extrapolators of length $N = 25$. In Figures 4.5 and 4.6 the zoomed sections of area (lateral position, $3200 - 8000$ m; depth, $1950 - 2990$ m) are shown. Figures 4.5a-c show zoomed migrated sections of the non-weighted filters, while Figures 4.6a-c show migrated sections for the weighted case. Clearly, the prestack depth migrated images using the compensating operators outperform those generated using non-compensating operators.

4.6 Comparsion

In this section the best results for compensating operators of L_1-error and L_1-norm are compared for $N = 25$. In Figure 4.8 both the algorithm results are shown by applying the compensating operators to the visco-acoustic data set. Both enhanced the migrated results at the higher depth. L_1-norm non-sparse version seems slightly more enhanced at depth but there are slightly more ringings. On the other hand the weighted L_1-error behave more robust and stable for the ringings. As the Marmousi model data set have depth of 3 km, the effect of ringing is not that much high. It will be more evident for larger depths. For larger depths, both the algorithms can become unstable but L_1-error will behave relatively better for larger depths. In the Figure 4.9 the corresponding zoomed section (lateral

position: $3200 - 8000$ m and depth: $1950 - 2990$ m) are shown.

4.7 Conlusions

In this chapter, the L_1-error (weighted and non-weighted) algorithm is discussed. For $N = 25$ L_1-error performs better than L_1-norm (both sparse and non-sparse). For weight selection, the method of Thorbecke in [10] is adapted. For selecting weights some adaptive algorithm can be utilized to ensure better performance. The error in filter responses shows that the weighted version of the design is performing better. If non-weighted version is special case of weighted designs. In case of L_1-error the ringings at higher depth are relatively low as compared to the L_1-norm.

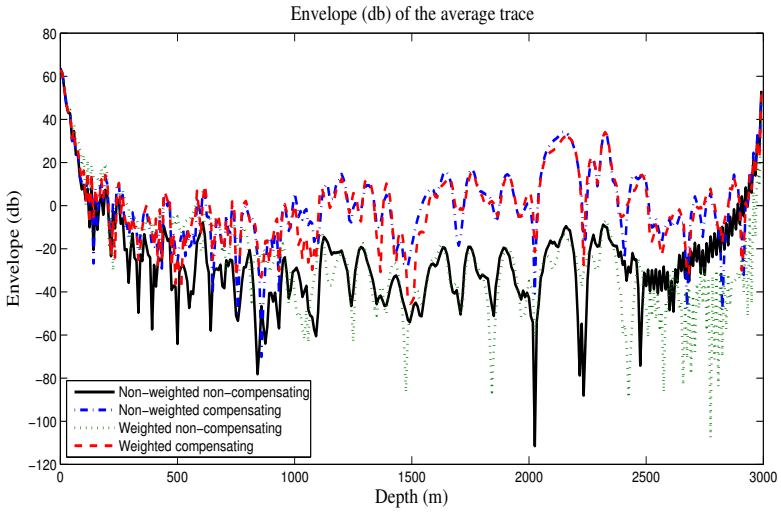

Figure 4.7: The envelopes of the average trace from images migrated using the proposed non-compensating and compensating weighted and non-weighted $f - x$ extrapolation filters with $N = 25$

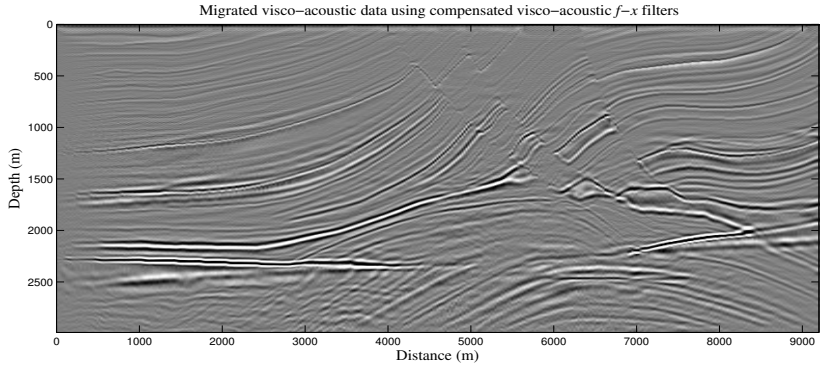

(a)

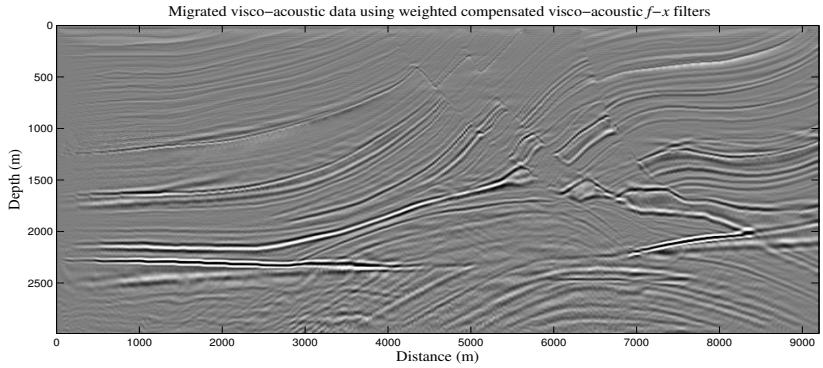

(b)

Figure 4.8: Migrated Marmousi images using the proposed compensating filters with $N = 25$. (a) shows image obtained from applying L_1-norm non-sparse $f - x$ extrapolation filters to visco-acoustic data set and (b) shows image obtained from applying weighted L_1-error $f - x$ extrapolation filters to visco-acoustic data set.

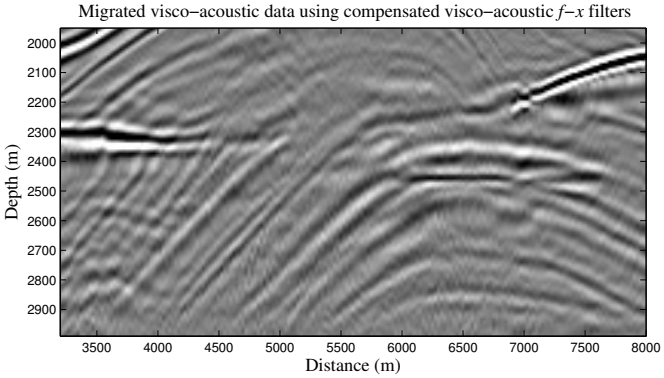

(a)

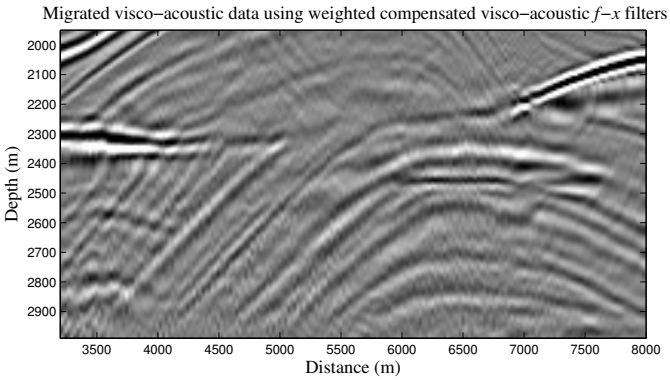

(b)

Figure 4.9: Zoom-in area of the migrated images using the proposed compensating filters with $N = 25$. (lateral position: $3200 - 8000$ m and depth: $1950 - 2990$ m). (a) shows image obtained from applying L_1-norm non-sparse $f - x$ extrapolation filters to visco-acoustic data set and (b) shows image obtained from applying weighted L_1-error $f - x$ extrapolation filters to visco-acoustic data set.

CHAPTER 5

CONCLUSIONS AND RECOMMENDATIONS

As in reality the seismic data has attenuating effect which should be compensated. As in past decades number of researcher assumed the data to be acoustic, those algorithms need to accommodate the compensating effect of visco-acoustic data. Two algorithms are used to design such filters which have this compensating effect. In result, enhanced resolution images are obtained as compared to non-compensating operators. L_1-norm has both sparse and non-sparse versions. Sparsity helps in improving the computational performance of the migration process. The second algorithm introduces the weighting effect, which helps in improving results using less number of coefficients. With weighting the required design results in better images and relatively low ringing effects.

The method discussed in this thesis can easily modify all the existing acoustic non-compensating filter designs to visco-acoustic compensating filter designs with

little effort. This method can also be extended to 2-D filters which are used to migrate 3-D seismic data. For 2-D filters design either use direct designing the 2-D filters or use McClellan transformation to extend 1-D filters to 2-D case.

Another approach to extend the work is to design operators for elastic and visco-elastic medium which are more realistic models. For that case 3D elastic and visco-elastic datasets are required. To generate acoustic, visco-acoustic, elastic and visco-elastic opensource codes can be used. Sofi2D can generate 2-D datasets and for 3-D case, Sofi3D can be used [34]. OpenSource codes from Dr. Jan Thorbcke can work only for 2-D data set generation. And for migration of 2-D and 3-D data sets using 1-D and 2-D filters, respectively, the functions of Dr. Thorbecke can be used [35].

REFERENCES

[1] O. Yilmaz, Ed., *Seismic Data Analysis: Processing, Inversion, and Interpretation of Seismic Data*, 2nd ed. Society of Exploration Geophysicists, 2001.

[2] R. P. Bording and L. R. Lines, *Seismic modeling and imaging with the complete wave equation*. Society of Exploration Geophysicists Tulsa, 1997.

[3] D. E. Dudgeon and R. M. Mersereau, "Multidimensional digital signal processing," 1990.

[4] B. Buttkus, *Spectral Analysis and Filter Theory in Applied Geophysics: With 23 Tables*. Springer Science & Business Media, 2000.

[5] D. Hale, "Stable explicit depth extrapolation of seismic wavefields," *Geophysics*, vol. 56, pp. 1770 – 1777, 1991.

[6] O. Holberg, "Towards optimum one-way wave propagation," *Geophysical Prospecting*, vol. 36, pp. 99–114, 1988.

[7] J. Thorbecke, "Common focus point technology," Ph.D. dissertation, Delft University of Technology, 1997.

[8] R. Soubaras, "Explicit 3-D migration using equiripple polynomial expansion and Laplace synthesis," *Geophysics*, vol. 61, no. 5, pp. 1386–1393, 1996.

[9] L. J. Karam and J. H. McClellan, "Efficient design of digital filters for 2-D and 3-D depth migration," *Signal Processing, IEEE Transactions on*, vol. 45, no. 4, pp. 1036–1044, April 1997.

[10] J. W. Thorbecke, K. Wapenaar, and G. Swinnen, "Design of one-way wavefield extrapolation operators, using smooth functions in WLSQ optimization," *Geophysics*, vol. 69, no. 4, pp. 1037–1045, 2004.

[11] W. A. Mousa, M. V. D. Baan, S. Boussakta, and D. McLernon, "Designing stable operators for explicit depth extrapolation of 2-D & 3-D wavefields using projections onto convex sets," *Geophysics*, vol. 74, no. 2, pp. P.S33–S45, March-April 2009.

[12] W. Mousa, "Imaging of the SEG/EAGE salt model seismic data using sparse–finite-impulse-response wavefield extrapolation filters," *Geoscience and Remote Sensing, IEEE Transactions on*, vol. 52, no. 5, pp. 2700–2714, 2014.

[13] M. M. Naseer and W. A. Mousa, "Linear complementarity problem : A novel approach to design finite-impulse response wavefield extrapolation filters," *Geophysics*, vol. 80, no. 2, pp. 1–9, 2015.

[14] R. Mittet, R. Sollie, and K. Hokstad, "Prestack depth migration with compensation for absorption and dispersion," *Geophysics*, vol. 60, no. 5, pp. 1485–1494, 1995.

[15] R. Mittet, "A simple design procedure for depth extrapolation operators that compensate for absorption and dispersion," *Geophysics*, vol. 72, no. 2, pp. S105–S112, 2007.

[16] J. G. Hagedoorn, "A process of seismic reflection interpretation," *Geophysical Prospecting*, vol. 2, no. 2, pp. 85–127, 1954.

[17] J. F. Clœrbout, "Imaging the earth's interior," 1982.

[18] E. A. Robinson and S. Treitel, *Geophysical signal analysis*. Prentice-Hall New Jersey, 1980, vol. 263.

[19] P. Kearey, M. Brooks, and I. Hill, *An introduction to geophysical exploration*. John Wiley & Sons, 2013.

[20] D. E. Dudgeon and R. M. Mersereau, "Multidimensional digital signal processing," *Prentice-Hall Signal Processing Series, Englewood Cliffs: Prentice-Hall, 1984*, vol. 1, 1984.

[21] L. J. Karam and J. H. McClellan, "Efficient design of digital filters for 2-d and 3-d depth migration," *Signal Processing, IEEE Transactions on*, vol. 45, no. 4, pp. 1036–1044, 1997.

[22] C. L. Liner, *Elements of 3D seismology*. PennWell Books, 2004, vol. 1.

[23] D. Bhardwaj, S. Yerneni, and S. Phadke, "Parallel computing in seismic data processing," in *3rd International Petroleum Conf. and Exhibition (PETROTECH-99)*. Citeseer, 1999, pp. 279–285.

[24] D. Hale, "Stable explicit depth extrapolation of seismic wavefields," *Geophysics*, vol. 56, no. 11, pp. 1770–1777, 1991.

[25] W. Rietveld and A. Berkhout, "Prestack depth migration by means of controlled illumination," *Geophysics*, vol. 59, no. 5, pp. 801–809, 1994.

[26] D. Mattera, F. Palmierl, and S. Haykin, "Efficient sparse fir filter design," in *Acoustics, Speech, and Signal Processing (ICASSP), 2002 IEEE International Conference on*, vol. 2. IEEE, 2002, pp. II–1537.

[27] T. Baran, D. Wei, and A. V. Oppenheim, "Linear programming algorithms for sparse filter design," *IEEE Transactions on Signal Processing*, vol. 58, no. 3, pp. 1605 – 1617, 2010.

[28] E. J. Candes, J. K. Romberg, and T. Tao, "Stable signal recovery from incomplete and inaccurate measurements," *Communications on pure and applied mathematics*, vol. 59, no. 8, pp. 1207–1223, 2006.

[29] H. Stark and Y. Yang, *Vector Space Projections: a numerical approach to Signal and Image processing, Neural nets, and Optics*, 1st ed. John Wiley and Sons Publisher, 1998.

[30] M. Grant and S. Boyd, "CVX: Matlab software for disciplined convex programming, version 2.1," Mar. 2014.

[31] E. J. Candè and M. B. Wakin, "An introduction to compressive sampling," *Signal Processing Magazine, IEEE*, vol. 25, no. 2, pp. 21–30, 2008.

[32] J. W. Thorbecke and D. Draganov, "Finite-difference modeling experiments for seismic interferometry," *Geophysics*, vol. 76, no. 6, pp. H1–H18, 2011.

[33] D. LiLin, X. Yue, C. Peng, W. Gang, and L. ShaoQian, "A low-complexity multiple signal representation scheme in downlink OFDM-CDMA," *Springer Sci China Ser F-Inf Sci*, vol. 52, no. 12, pp. 2433–2444, 2009.

[34] KIT-GPI, "Seismic modeling with finite differences 3D (SOFI3D)." [Online]. Available: https://www.gpi.kit.edu/SOFI3D.php

[35] J. W. Thorbecke and D. Draganov, "Finite-difference modeling experiments for seismic interferometry," *Geophysics*, vol. 76, no. 6, pp. H1–H18, 2011.

Vitae

- Name: Syed Abdul Salam
- Nationality: Pakistani
- Date of Birth: 01-January-1988
- Email: *creativesalam@gmail.com*
- Permenant Address: Rang Mohallah Mingora Swat, Khyber Pukhtoonkhwa, Pakistan

  I did my B.Sc Electrical Engineering from University of Engineering and Technology (UET) Peshawar, Pakistan in 2010. After my undergraduate studies, I joined Center for Intelligent Systems and Networks Research (CISNR), UET Peshawar for one year as a Research Assistant. Then I worked in UET Peshawar as a Lecturer for two years.

LIST OF PUBLICATIONS

- **Syed Abdul Salam** and Wail A. Mousa, "The Design of Sparse L_1-norm Visco-Acoustic Wavefield Extrapolators", submitted to *Geophysics*

- **Syed Abdul Salam** and Wail A. Mousa, "The Design of Visco-Acoustic Weighted L_1-error Frequency-Space Wavefield Extrapolators", submitted to *Geophysical Prospecting*